MucosalImmunology

www.nature.com/mi

ARTICLE OPEN

Plectin ensures intestinal epithelial integrity and protects colon against colitis

Alzbeta Krausova[1], Petra Buresova[1,2], Lenka Sarnova[1], Gizem Oyman-Eyrilmez[1], Jozef Skarda[3,4], Pavel Wohl[5], Lukas Bajer[5], Eva Sticova[6,7], Lenka Bartonova[6], Jiri Pacha[8], Gizela Koubkova[9], Jan Prochazka[9,10], Marina Spörrer[11], Christopher Dürrbeck[11], Zuzana Stehlikova[12], Martin Vit[13], Natalia Ziolkowska[14], Radislav Sedlacek[9,10], Daniel Jirak[15,16], Miloslav Kverka[12], Gerhard Wiche[17], Ben Fabry[11], Vladimir Korinek[18] and Martin Gregor[1]

Plectin, a highly versatile cytolinker protein, provides tissues with mechanical stability through the integration of intermediate filaments (IFs) with cell junctions. Here, we hypothesize that plectin-controlled cytoarchitecture is a critical determinant of the intestinal barrier function and homeostasis. Mice lacking plectin in an intestinal epithelial cell (IEC; $Ple^{\Delta IEC}$) spontaneously developed colitis characterized by extensive detachment of IECs from the basement membrane (BM), increased intestinal permeability, and inflammatory lesions. Moreover, plectin expression was reduced in the colons of ulcerative colitis (UC) patients and negatively correlated with the severity of colitis. Mechanistically, plectin deficiency in IECs led to aberrant keratin filament (KF) network organization and the formation of dysfunctional hemidesmosomes (HDs) and intercellular junctions. In addition, the hemidesmosomal α6β4 integrin (Itg) receptor showed attenuated association with KFs, and protein profiling revealed prominent downregulation of junctional constituents. Consistent with the effects of plectin loss in the intestinal epithelium, plectin-deficient IECs exhibited remarkably reduced mechanical stability and limited adhesion capacity in vitro. Feeding mice with a low-residue liquid diet that reduced mechanical stress and antibiotic treatment successfully mitigated epithelial damage in the $Ple^{\Delta IEC}$ colon.

Mucosal Immunology _####################_; https://doi.org/10.1038/s41385-021-00380-z

INTRODUCTION

The intestinal epithelium is composed of a single layer of tightly linked intestinal epithelial cells (IECs), forming a selective physical barrier that is critical for gut homeostasis. A breach in the intestinal barrier, referred to as "leaky gut"[1], results in excessive exposure to luminal microbiota and in a concomitant innate immune response. Subsequent dysregulation of the finely-tuned interplay among gut microbiota, IECs, and immune cells accounts for uncontrolled inflammation and pathogenesis of intestinal disorders such as inflammatory bowel disease (IBD) and colorectal cancer (CRC)[2,3].

The epithelial barrier function is secured by cell junctions that seal intercellular spaces and interlink IECs with the underlying basement membrane (BM) into a structural and functional continuum. Alterations in junctional proteins and BM components may lead to a breakdown of the barrier, and genetic studies identified multiple links between junction/BM-associated genes and the development of IBD[4–6]. While apical tight junctions (TJs) and subjacent adherens junctions (AJs) confer paracellular transport selectivity, desmosomes (Ds) together with BM-linked hemidesmosomes (HDs) provide the intestinal epithelium with resilience to mechanical stress generated by intestinal peristalsis[7]. It is noteworthy that recently reported mouse models demonstrate the protective role of Ds and HDs in the context of both intestinal inflammation[8,9] and colitis-associated CRC[8]. Accumulating evidence suggests that fundamental features of Ds and HDs (such as stability, dynamics, and mechanotransduction capacity) heavily rely on their interconnection with keratin filament (KF) networks[10,11]. This places plakins[12], a family of cytolinker proteins mediating physical linkage between KFs and cell junctions, at the very center of the processes controlling epithelial homeostasis.

[1]Laboratory of Integrative Biology, Institute of Molecular Genetics of the Czech Academy of Sciences, Prague, Czech Republic; [2]Department of Cell Biology, Faculty of Science, Charles University, Prague, Czech Republic; [3]Department of Clinical and Molecular Pathology, Faculty of Medicine and Dentistry, Palacky University and University Hospital in Olomouc, Olomouc, Czech Republic; [4]Institute of Pathology, University Hospital Ostrava, Ostrava, Czech Republic; [5]Department of Gastroenterology and Hepatology, Institute for Clinical and Experimental Medicine, Prague, Czech Republic; [6]Department of Clinical and Transplant Pathology, Institute for Clinical and Experimental Medicine, Prague, Czech Republic; [7]Department of Pathology, Third Faculty of Medicine, Charles University, Prague, Czech Republic; [8]Department of Epithelial Physiology, Institute of Physiology of the Czech Academy of Sciences, Prague, Czech Republic; [9]Czech Centre for Phenogenomics, Institute of Molecular Genetics of the Czech Academy of Sciences, Prague, Czech Republic; [10]Laboratory of Transgenic Models of Diseases, Institute of Molecular Genetics of the Czech Academy of Sciences, Prague, Czech Republic; [11]Department of Physics, University of Erlangen-Nuremberg, Erlangen, Germany; [12]Laboratory of Cellular and Molecular Immunology, Institute of Microbiology of the Czech Academy of Sciences, Prague, Czech Republic; [13]University of Liberec, Faculty of Mechatronics Informatics and Interdisciplinary Studies, Liberec, Czech Republic; [14]Institute of Biophysics and Informatics, First Faculty of Medicine, Charles University, Prague, Czech Republic; [15]Technical University of Liberec, Faculty of Health Studie, Liberec, Czech Republic; [16]Department of Radiodiagnostic and Interventional Radiology, Institute for Clinical and Experimental Medicine, Prague, Czech Republic; [17]Department of Biochemistry and Cell Biology, Max F. Perutz Laboratories, University of Vienna, Vienna, Austria and [18]Laboratory of Cell and Developmental Biology, Institute of Molecular Genetics of the Czech Academy of Sciences, Prague, Czech Republic

Correspondence: Martin Gregor (martin.gregor@img.cas.cz)

These authors contributed equally: Alzbeta Krausova, Petra Buresova.

Received: 24 August 2020 Revised: 6 January 2021 Accepted: 11 January 2021
Published online: 05 March 2021

Plectin, a highly versatile member of the plakin protein family, crosslinks intermediate filaments (IFs) of different types and anchors them at cellular junctions, including HDs and Ds of epithelial cells[13]. Multiple mutations in the *plectin* gene have been identified in epidermolysis bullosa (EB)[14], a disorder characterized by excessive blister formation in skin[15,16] with reported cases of concurrent IBD[17,18]. Previous studies have shown that plectin ablation disrupts highly organized epithelial KF networks and alters the structure and functionality of cell junctions[19–22]. For example, tissue-specific deletion of *plectin* in the mouse biliary epithelium has adverse effects on the formation of TJs, AJs, and Ds, with deleterious consequences for epithelial stability under cholestasis[22]. Likewise, analysis of knock-in mice recapitulating dominant EB simplex suggests that HD stability in basal keratinocytes depends on plectin-mediated recruitment of KFs[20]. Mechanistically, dysfunctional HDs account for epithelial fragility and lesional defects[23] which resemble those seen in patients with IBD[24]. Although these observations suggest a linkage between plectin dysfunction and intestinal pathologies, plectin's role in the intestinal epithelium remains unaddressed.

In this study, we found that plectin expression was reduced in patients with active ulcerative colitis (UC) and that plectin expression levels negatively correlated with the severity of colitis. To study the underlying molecular mechanisms, we generated two new mouse lines: one constitutive ($Ple^{\Delta IEC}$) and the other with tamoxifen (TMX)-inducible ($Ple^{\Delta IEC\text{-}ERT2}$) plectin ablation in IECs. The phenotypic characterization of these mice demonstrated that loss of plectin leads to spontaneous development of a colitic phenotype characterized by extensive detachment of IECs from the BM, increased intestinal permeability, and formation of inflammatory lesions. These results demonstrate the absolute indispensability of plectin for the maintenance of intestinal epithelium integrity, and moreover that both mouse lines provide a useful model system for investigating disease etiology and testing palliative therapies.

RESULTS

Suppression of plectin in human patients with UC

To examine the role of plectin in the pathogenesis of UC, we screened for potential alterations of plectin expression in a cohort of ~100 UC patients. The analysis of immunolabeled biopsy samples taken from patients and healthy controls revealed discontinuous and rather patchy plectin staining patterns in UC biopsies. The gaps in the plectin staining pattern coincided with goblet cell openings heavily loaded with mucus. In healthy controls, plectin decorated both apical and basal membranes of IECs evenly (Figs. 1A and S1A), resembling plectin localization in mouse intestinal sections (Fig. S1B and published previously[25]). In addition, mRNA profiling showed significantly reduced expression levels of plectin in biopsies from patients with active UC (Fig. 1B). Histological analysis revealed that low mRNA levels of plectin were associated with higher inflammation (Fig. 1C) and higher C reactive protein levels in serum (not shown).

IEC-specific plectin-deficient mice develop a colitic phenotype due to intestinal barrier dysfunction

To explore the role of plectin in the intestinal epithelium in greater detail, we generated IEC-specific *plectin* knockout ($Ple^{\Delta IEC}$) mice. Successful ablation of plectin in IECs was confirmed by immunofluorescence microscopy (Fig. S1C). The newly generated $Ple^{\Delta IEC}$ mice had a considerably lower bodyweight (Figs. 1D and S1D), suffered from persistent diarrhea with occasional rectal bleeding (Fig. S1E, and not shown), and frequently developed rectal prolapse (Fig. 1E). As the onset and progression of UC correlate with defects in the intestinal barrier function[26,27], we assessed barrier integrity either by ex vivo measurements of intestinal transepithelial electrical resistance (TEER) or by in vivo orogastric gavage of FITC-dextran. We observed significantly lower TEER in the proximal and distal colon regions of 12-week-old $Ple^{\Delta IEC}$ compared to $Ple^{fl/fl}$ mice. Moreover, TEER values in $Ple^{fl/fl}$ mice were three-times higher in their distal parts than in their proximal parts; by contrast, TEER values in $Ple^{\Delta IEC}$ mice were equally low in distal and proximal colon segments (Fig. 1F). Compared to $Ple^{fl/fl}$ mice, $Ple^{\Delta IEC}$ mice consistently displayed a higher penetration rate of FITC-dextran into blood already at 4 weeks, and this difference became even more apparent in older animals (Fig. 1G).

In addition, a histological inspection of hematoxylin-eosin (H&E)-stained colon sections revealed extensive translocation of luminal bacteria into $Ple^{\Delta IEC}$ mucosa in 30-week-old mice (Fig. 1H). Given the hampered barrier function in the $Ple^{\Delta IEC}$ intestine, we screened $Ple^{fl/fl}$ and $Ple^{\Delta IEC}$ mice for signs of inflammation. Chemiluminescence-based whole body imaging[28] showed positive abdominal areas in $Ple^{\Delta IEC}$ mice (Fig. 1I), which correlated strongly with significantly higher myeloperoxidase activity (MPO; Fig. 1J). Moreover, mild inflammation of the $Ple^{\Delta IEC}$ colon was confirmed by increased immune cell infiltration, extent (or intensity) of acute/chronic inflammation, and lymphatic follicle size (Figs. 1K, L and S2A), and a higher percentage of edema and ulceration indicated higher epithelial damage (Fig. S2B). Together, these results suggest that plectin is critical for the maintenance of the intestinal barrier and thus could be directly linked to the onset and progression of UC.

Loss of plectin leads to hyperproliferation and aberrant differentiation of IECs

Further histological inspection of H&E-stained colonic sections revealed thickening of the colonic mucosa and significant crypt damage with excessive sloughing of IECs detached from the subjacent BM in plectin-deficient specimens (Fig. 2A). In addition, the colon of $Ple^{\Delta IEC}$ mice showed a higher rate of proliferation as determined from Ki-67-stained sections (Fig. 2B). Consistently, an increase in the number of proliferating transit-amplifying IECs in the crypts of $Ple^{\Delta IEC}$ animals was evident from BrdU incorporation assessed 2, 24, and 48 h after a BrdU pulse (Fig. 2C). Interestingly, TUNEL staining indicated a minimal degree of spontaneous apoptosis in both $Ple^{fl/fl}$ and $Ple^{\Delta IEC}$ mice (Fig. S3A). In parallel with the prominent hyperplasia, the $Ple^{\Delta IEC}$ colon contained a higher proportion of PAS-positive goblet cells (Fig. 2D), corresponding to a higher mucus discharge (Fig. 2E). Immunolabeled $Ple^{\Delta IEC}$ colonic sections also showed a lower percentage of chromogranin A (ChgA)-positive enteroendocrine cells (Fig. S3B) and an extended keratin 20 (K20)-positive zone (Fig. S3C). Similar, albeit less pronounced, trends were observed in the $Ple^{\Delta IEC}$ small intestine (Fig. S4). Plectin deficiency thus results in hyperproliferation and aberrant differentiation of IECs, affecting the spatiotemporal organization of the intestinal epithelium.

Plectin-deficient IECs form aberrant cell junctions and disordered KF networks

As the structural and functional integrity of epithelia is secured by cell junctions[2,29], we compared the morphology of cell-ECM (HDs) and cell–cell (TJs, AJs, and Ds) adhesions formed by $Ple^{fl/fl}$ and $Ple^{\Delta IEC}$ IECs, using transmission electron microscopy (TEM). A quantitative analysis of the HD size revealed an extended cross-sectional length of seemingly less electrodense HD plaques in the $Ple^{\Delta IEC}$ colon; furthermore, the space between HDs and the BM was significantly dilated (Fig. 3A). Similar to HDs, we also found significantly dilated intercellular spaces of TJs, AJs, and Ds between adjacent $Ple^{\Delta IEC}$ IECs (Fig. 3A). These morphological alterations coincided with generally lower expression levels of the hemidesmosomal constituents Itgα6 and Itgβ4 and the following cell–cell junctional markers: zonula occludens 1 (ZO-1; TJs), E-cadherin (E-cad; AJs), desmoglein 2 (Dsg2; Ds), and desmoplakin 1/2 (Dsp1/2; also Ds) at both mRNA and protein levels (Fig. 3B–E).

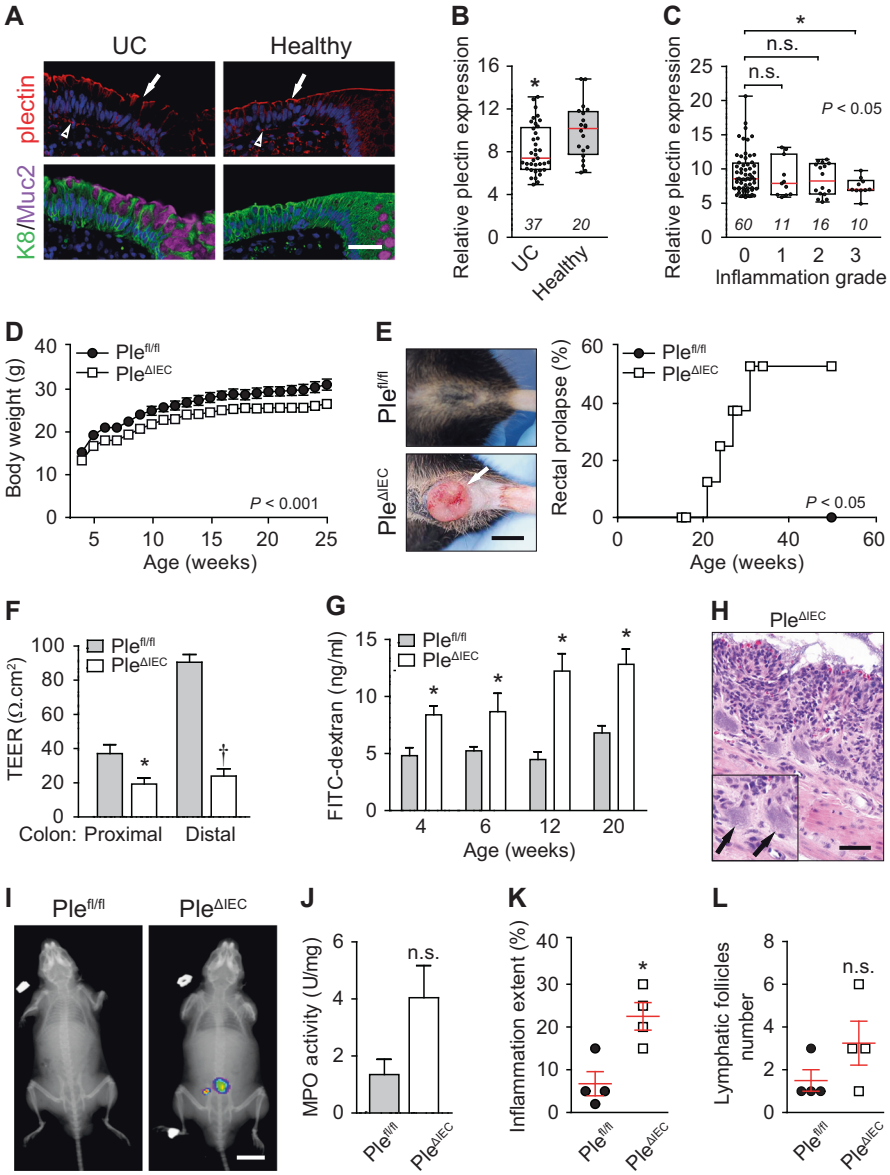

Fig. 1 Loss of plectin is associated with UC in human patients and leads to intestinal epithelial barrier dysfunction with concomitant inflammation in mouse. A Paraffin-embedded colon sections from UC patients (UC) and healthy controls (healthy) were immunolabeled with antibodies to plectin (red), keratin 8 (K8; green), and mucin 2 (Muc2; magenta). Nuclei were stained with Hoechst (blue). Arrows, apical IEC membrane; arrowheads, basal IEC membrane. Scale bar, 40 µm. **B** Relative *plectin* mRNA levels in rectum biopsies collected from healthy controls and patients with active UC. Scattered boxplots show individual data points, median, 25th, and 75th percentile with whiskers reaching the last data point. The numbers of included participants per cohort are indicated in the graph. **C** Relative *plectin* mRNA expression in rectum biopsies collected from UC patients clustered based on inflammation scored in H&E-stained rectum sections. Scattered boxplots show individual data points, median, 25th, and 75th percentile with whiskers reaching the last data point. The numbers of included participants per cohort are indicated in the graph. **D** Bodyweight of $Ple^{fl/fl}$ and $Ple^{\Delta IEC}$ mice was monitored for 25 weeks, $n = 7$. **E** Representative images of the rectum of 30-week-old $Ple^{fl/fl}$ and $Ple^{\Delta IEC}$ mice. Kaplan–Meier graph shows age-related rectal prolapse incidence. **F** Intestinal transepithelial electrical resistance (TEER) measured ex vivo in both proximal and distal colons of 12-week-old $Ple^{fl/fl}$ and $Ple^{\Delta IEC}$ mice, $n = 4$. **G** In vivo permeability of mucosa of $Ple^{fl/fl}$ and $Ple^{\Delta IEC}$ mice (at the age indicated) measured by monitoring 40-kDa FITC-dextran levels in plasma 4 h after orogastric gavage, $n = 3$–7. **H** Representative image of $Ple^{\Delta IEC}$ colon section from 30-week-old $Ple^{\Delta IEC}$ mouse stained with H&E. Arrows, bacterial patches in the mucosa. Scale bar, 50 µm. **I** In vivo chemiluminescence images of 12-week-old $Ple^{\Delta IEC}$ and $Ple^{fl/fl}$ mice injected with myeloperoxidase (MPO) inflammation probe. **J** MPO activity (a marker of neutrophil infiltration) measured in colon lysates from 12-week-old $Ple^{\Delta IEC}$ and $Ple^{fl/fl}$ mice, $n = 3$. **K**, **L** Inflammation extent (percentage) (**K**) and the number of lymphatic follicles (**L**) assessed from H&E-stained sections of 12-week-old $Ple^{fl/fl}$ and $Ple^{\Delta IEC}$ colons, $n = 4$. Data are presented as mean ± SEM, n.s. not significant, $^{*}P < 0.05$, $^{**}P < 0.01$, $^{\dagger}P < 0.001$.

These results clearly show that plectin deficiency leads to the formation of aberrant intestinal junctional complexes, which likely accounts for breached epithelial barrier integrity.

In previous studies, we showed that plectin controls cell junctions through anchorage of IF networks[20,22,30]. Therefore, we next compared the appearance of KFs in $Ple^{fl/fl}$ and $Ple^{\Delta IEC}$ colon sections using immunofluorescence microscopy. Although the general appearance of K8 and K19 networks did not significantly differ in the two cell types (Fig. S5), super-resolution microscopy of pan-K-labeled sections revealed less pronounced apical staining of $Ple^{\Delta IEC}$ IECs (Fig. 4A). Moreover, in $Ple^{\Delta IEC}$ IECs, pan-K positive filaments formed less-ordered and rather coarse meshworks, while

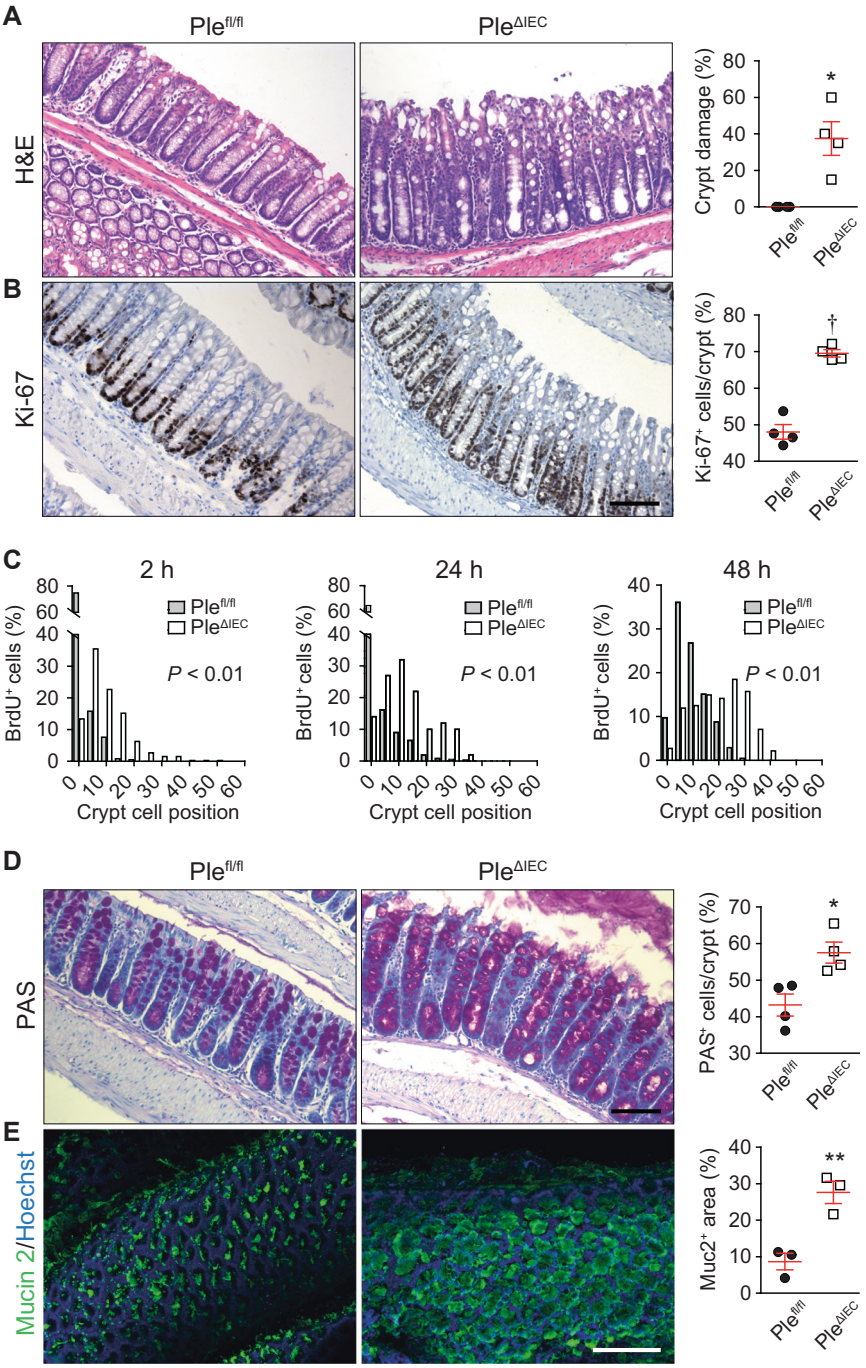

Fig. 2 Plectin-deficient IECs exhibit aberrant proliferation and differentiation, resulting in altered crypt organization. A, **B** Representative images of H&E staining (**A**) and Ki-67 immunohistochemistry (proliferating cells) (**B**) of *Ple*$^{fl/fl}$ and *Ple*$^{\Delta IEC}$ paraffin-embedded colon sections. Scale bar, 100 µm. Graphs show quantification of colonic crypt damage given as a percentage of crypts with >5% of IECs detached from BM (**A**) and percentage of the Ki-67-positive (Ki-67$^+$) IECs per crypt (**B**), $n = 3$–4. **C** Histograms showing the percentage of BrdU-positive (BrdU$^+$) cells in given positions of *Ple*$^{fl/fl}$ and *Ple*$^{\Delta IEC}$ colonic crypts at 2, 24, and 48 h after BrdU pulse. Cells were numbered sequentially from crypt base to lumen, with cell position 0 assigned to the first cell at the base of each crypt. At least nine crypts per mouse were analyzed from three mice per time point and genotype. **D**, **E** Representative images of PAS staining (goblet cells) (**D**) and mucin-2 (Muc2) immunofluorescence in mucus layer (**E**) of *Ple*$^{fl/fl}$ and *Ple*$^{\Delta IEC}$ distal colon sections (**D**) and colon whole mounts (**E**). Scale bars, 100 µm (**D**), and 200 µm (**E**). Graphs show quantification of percentage of PAS-positive (PAS$^+$) IECs per crypt (**D**) and percentage of mucin-2-positive (Muc2$^+$) area per whole mount area examined (**E**), $n = 3$–4. Data are presented as mean ± SEM, $^*P < 0.05$, $^{**}P < 0.01$, $^{\dagger}P < 0.001$.

Ple$^{fl/fl}$ IECs displayed typical staining patterns with filaments regularly aligned along the apicobasal axis (Fig. 4A). The changes in KF network organization were not caused by altered keratin (K8, K18, and K19) expression, as no differences were found at either the mRNA or the protein level (Fig. 4B, C). No apparent abnormalities were seen in actin filament and microtubule organization (Figs. S5 and S6A).

Aberrant KF cytoarchitecture was also clearly discernible in pan-K immunolabeled monolayers of plectin-deficient (KO) human IECs (Caco-2). To mimick the in vivo situation, mature

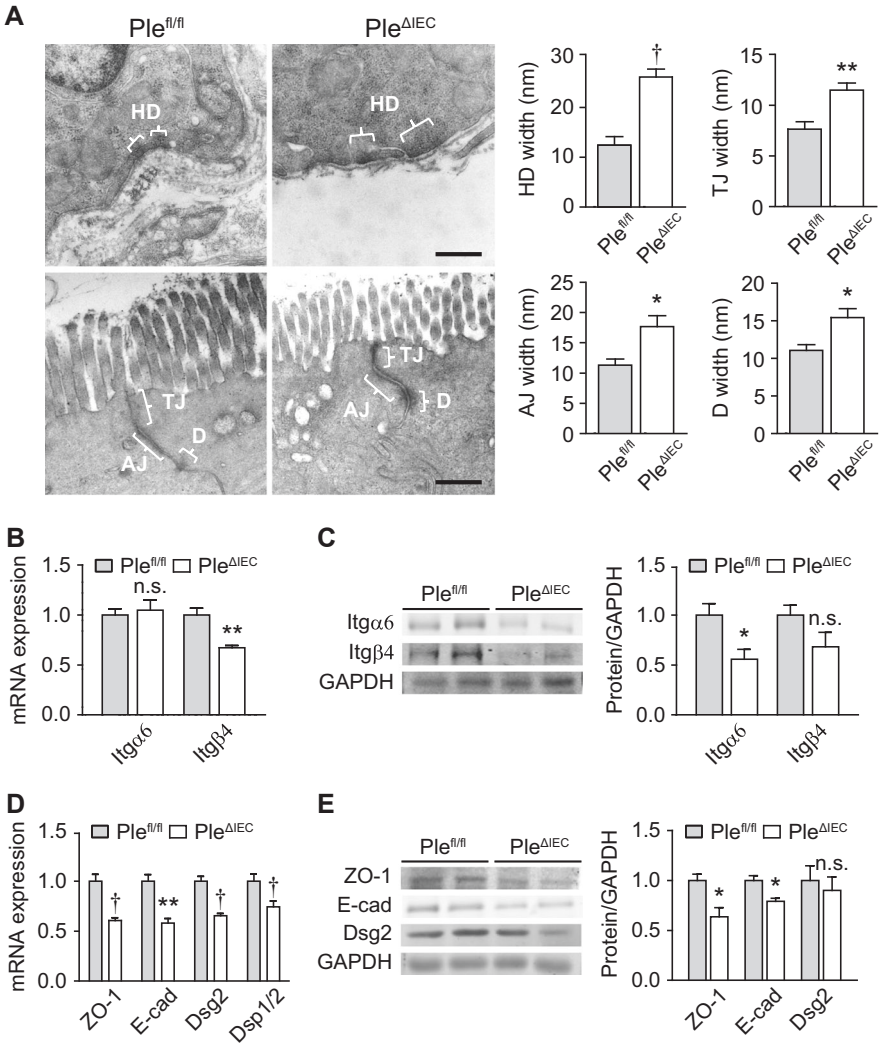

Fig. 3 Formation of aberrant cell junctions in *Ple*$^{\Delta IEC}$ IECs. A Representative TEM micrographs of *Ple*$^{fl/fl}$ and *Ple*$^{\Delta IEC}$ IEC junctional complexes. Braces (white) indicate hemidesmosomes (HD), tight junctions (TJ), adherens junctions (AJ), and desmosomes (Ds). Scale bar, 500 nm. Graphs show quantitative analyses of junctional complex widths (measured as the distance from IEC to BM (HD) or distance from IEC to IEC membrane (TJ, AJ, and Ds)). Five to fifteen junctions were measured (two mice per genotype). **B** Relative mRNA levels of integrin (Itg) α6 and β4 in scraped mucosa from *Ple*$^{fl/fl}$ and *Ple*$^{\Delta IEC}$ distal colons, $n = 4–5$. **C** Quantification of Itgβ4 and Itgα6 in scraped distal colon mucosa from *Ple*$^{fl/fl}$ and *Ple*$^{\Delta IEC}$ mice by immunoblotting. GAPDH, loading control. The graph shows relative band intensities normalized to average *Ple*$^{fl/fl}$ values, $n = 3$. **D** Relative mRNA levels of ZO-1, E-cadherin (E-cad), desmoglein 2 (Dsg2), and desmoplakin 1/2 (Dsp1/2) in *Ple*$^{fl/fl}$ and *Ple*$^{\Delta IEC}$ distal colons, $n = 5$. **E** Quantification of ZO-1, E-cad, and Dsg2 in *Ple*$^{fl/fl}$ and *Ple*$^{\Delta IEC}$ colon mucosa by immunoblotting. GAPDH, loading control. The graph shows relative band intensities normalized to average *Ple*$^{fl/fl}$ values, $n = 3$. Data are presented as mean ± SEM, n.s. not significant, $^{*}P < 0.05$, $^{**}P < 0.01$, $^{\dagger}P < 0.001$.

differentiated Caco-2 cells 16 days after the confluency were used. In wild-type (WT) cells, the KF network was densely packed around the cell center, from which individual KFs extended towards the cell periphery delineated by clearly defined desmoplakin-positive Ds (Fig. 4D). In contrast, KO cells showed tangled KFs, which were evenly distributed throughout the cytoplasm and seemingly overlapped with rather continuous desmoplakin-positive structures at the cell–cell borders (Fig. 4D). Similar to *Ple*$^{\Delta IEC}$ IECs, actin organization in KO cells appeared inconspicuous (Fig. S6B). Collectively, these findings indicate that plectin ablation in IECs results in altered keratin network organization and aberrant KF anchorage to desmosomal junctions.

Plectin preserves intestinal epithelial integrity through HD stabilization

Plectin-mediated attachment of the keratin network to Itgα6β4-containing HDs plays a crucial role in stabilizing the adhesion of keratinocytes to the matrix and hence imparts mechanical stability to the skin[20,31]. To examine whether the *Ple*$^{\Delta IEC}$ intestine phenotypically follows the same paradigm, we scrutinized colon and small intestine sections immunolabeled for K8 and Itgα6 (Fig. 5A) or collagen (Col) IV (Fig. S7). In line with the observations from H&E- and Sirius red-stained colon sections (Figs. 2A and S7), *Ple*$^{\Delta IEC}$ IECs partially lost their polarized orientation (Fig. S8A–C); they were misaligned and largely detached from the BM at the luminal surface of the crypts (Fig. 5A, upper panels). Despite a partial loss of apicobasal polarity of *Ple*$^{\Delta IEC}$ IECs (Fig. S8A–C), the epithelium retained a characteristic polarized distribution of the apical markers villin and ezrin (Fig. S8D, E). The extensive detachment of *Ple*$^{\Delta IEC}$ IECs was even more apparent in the small intestine, where we often found the whole epithelial sheet physically separated from underlying structures (Fig. 5A, lower panels). Remarkably, in both the *Ple*$^{\Delta IEC}$ colon and the small intestine, Itgα6-positive patches remained confined to the BM,

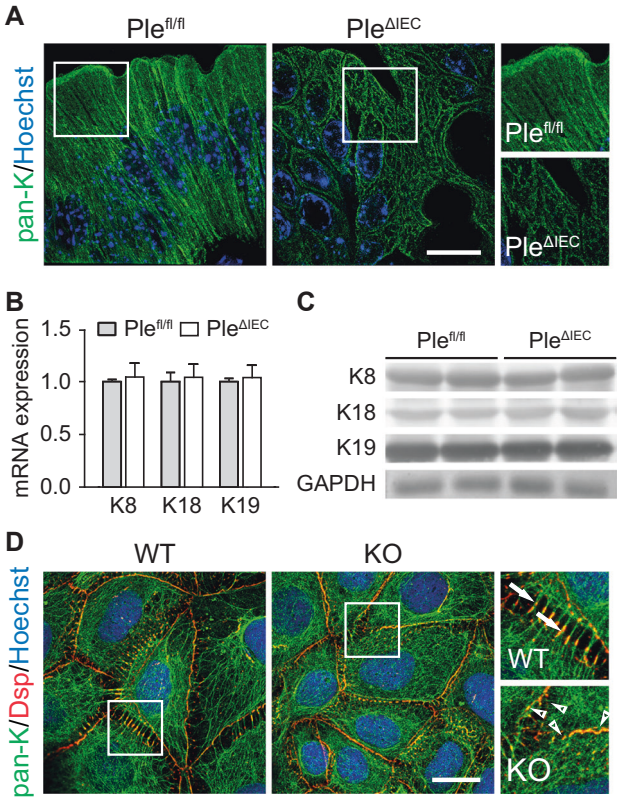

Fig. 4 Plectin organizes KFs in IECs. A Representative super-resolution STED images of $Ple^{fl/fl}$ and $Ple^{\Delta IEC}$ distal colon sections immunolabeled for pan-keratin (pan-K; green) with nuclei stained with Hoechst (blue). Scale bar, 10 µm. Boxed areas show ×1.3 images. **B**, **C** Relative mRNA (**B**) and protein (**C**) levels of K8, 18, and 19 in $Ple^{fl/fl}$ and $Ple^{\Delta IEC}$ distal colon, $n = 3–5$. Data are presented as mean ± SEM, $P > 0.05$ by unpaired Student t test. **D** Representative immunofluorescence images of WT and KO Caco-2 cell monolayer cultures immunolabeled for pan-K (green) and desmoplakin (Dsp; red). Nuclei were stained with Hoechst (blue). Arrows, straight K8 filaments anchored to Dsp-positive desmosomes; arrowheads, tangled K8 filaments. Scale bar, 20 µm. Boxed areas show ×2.5 images.

while detached IECs were entirely devoid of Itgα6 signals. Thus we conclude that plectin ablation abrogates the functional link between KFs and HDs.

To address the effects of plectin ablation biochemically, we prepared keratin-enriched cell fractions[19] from human WT and KO IEC Caco-2 lines and compared their integrin (Itg) content by immunoblotting using antibodies to Itgβ4. As expected, such cell fractions were highly enriched in keratins 8 (Fig. 5B), 18, and 19 (not shown). Although Itgβ4 levels were comparable in cell lysates, the Itgβ4 content of insoluble keratin fractions was significantly reduced in KO cells compared to WT cells (Fig. 5B). These observations correlated well with the histological data (Fig. 5A).

To assess whether plectin deficiency affects the biomechanical properties of IECs, we performed a series of quantitative assays with human IEC lines Caco-2 and hCC. Monitoring cell viability under mechanical stress on a stretched flexible membrane (uniaxial cyclic stretch) revealed the higher mechanical vulnerability of both KO cell lines, as the proportion of PI-positive (dead) cells significantly increased with stretch amplitudes ranging from 10% to 50% (Figs. 5C and S9A). Reduced mechanical resistance of KO cells was confirmed by fluid shear stress assay using a spinning disc device. When exposed to constant radial flow, KO cells displayed death rates about twice as high as that of their WT counterparts (Figs. 5D and S9B). Moreover, the fraction of detached Caco-2 (but not hCC) cells was higher for KO than WT cells. This suggests that plectin ablation weakens their adhesion to the underlying substratum.

To confirm this hypothesis, we quantified adhesion strength between ECM-coated superparamagnetic beads and cell adhesions using magnetic tweezers. We applied increasing forces of up to 15 nN to magnetic beads (force increase at 1 nN/s) and recorded the force at which each bead detached from the cell. From a total of >100 detachment events for each cell type, we calculated the cumulative detachment probability as a function of pulling force and report the force at which 50% of the beads detached from the cells (Figs. 5E and S9C). We measured lower detachment forces in both Caco-2 and hCC KO compared to WT cells, which confirms our hypothesis of weaker Itg-mediated adhesions in plectin-deficient cells. Hence, like for skin type I HDs[20], plectin loss is deleterious for the stability of type II HDs present in the intestine, leading to compromised mechanical resilience of IECs and intestinal epithelia.

IEC-specific plectin deficiency exacerbates experimental colitis

The spontaneous colitic phenotype in $Ple^{\Delta IEC}$ mice (Fig. 1) suggests that plectin deletion can contribute substantially to the pathogenesis of UC. To assess whether loss of plectin increases the susceptibility to colitis, we induced experimental colitis in $Ple^{fl/fl}$ and $Ple^{\Delta IEC}$ mice. Even a short exposure (3–4 days) to low DSS doses (1.5–2%) resulted in a dramatic bodyweight loss of $Ple^{\Delta IEC}$ mice, in sharp contrast to similarly treated $Ple^{fl/fl}$ which experienced only insignificant weight losses (Fig. 6A). The weight loss of mutant mice was associated with a higher disease activity index (DAI; Fig. 6A), a decreased survival rate (not shown), and a significant reduction in colon length (Fig. 6B). The severity of induced colitis in $Ple^{\Delta IEC}$ mice coincided with larger inflamed areas at days 4 and 6 after the initiation of DSS-treatment (Fig. 6C), corresponding to a higher influx of MPO-positive neutrophils and intestinal epithelial injury. Further, histological evaluation of "Swiss rolls" of the entire colon confirmed these results and revealed clear signs of inflammation and epithelial damage in all DSS-treated animals. However, large regions with heavy ulceration, crypt damage, and inflammatory response in $Ple^{\Delta IEC}$ mice were in striking contrast to fewer lesions in $Ple^{fl/fl}$ mice (Figs. 6D and S10A).

Since gut microbial dysbiosis is a typical finding in UC patients[32–34], we compared the composition of fecal microbiota in unchallenged $Ple^{fl/fl}$ and $Ple^{\Delta IEC}$ mice at the ages of 4, 12, and 20 weeks. Surprisingly, despite the impaired intestinal barrier and concomitant inflammation phenotype of $Ple^{\Delta IEC}$ mice (Fig. 1F–L), we observed no significant differences in alpha (Fig. S10B) and beta (Fig. 6E) diversities between both genotypes. In all animals, bacterial microbiota was dominated by bacteria belonging to families S24-7 (bacteroidetes), lactobacillaceae (firmicutes), and lachnospiraceae (firmicutes) (Fig. 6F). Together, these data show higher susceptibility of $Ple^{\Delta IEC}$ mice to DSS-induced colitis, accompanied by severe epithelial damage and inflammation in the absence of microbial dysbiosis.

Reduced mechanical stability of epithelia accounts for intestinal injury in $Ple^{\Delta IEC}$ mice

To identify the onset and time course of intestinal injury in $Ple^{\Delta IEC}$ mice, we assessed intestinal epithelial damage scores in newborn, 21-day-old, and 12-week-old mice (Figs. S11A and 7A–C). While newborn mice were histologically inconspicuous, the colon and the small intestine displayed first signs of damage in 21-day-old $Ple^{\Delta IEC}$ mice (see also Fig. S12B), which coincided with weaning and transition to solid chow. The onset of the epithelial breach was accompanied by the subsequent development of inflammatory response as shown by increased immune cell infiltration, extent (or intensity) of inflammation, and lymphatic follicle number/size (Fig. S12A).

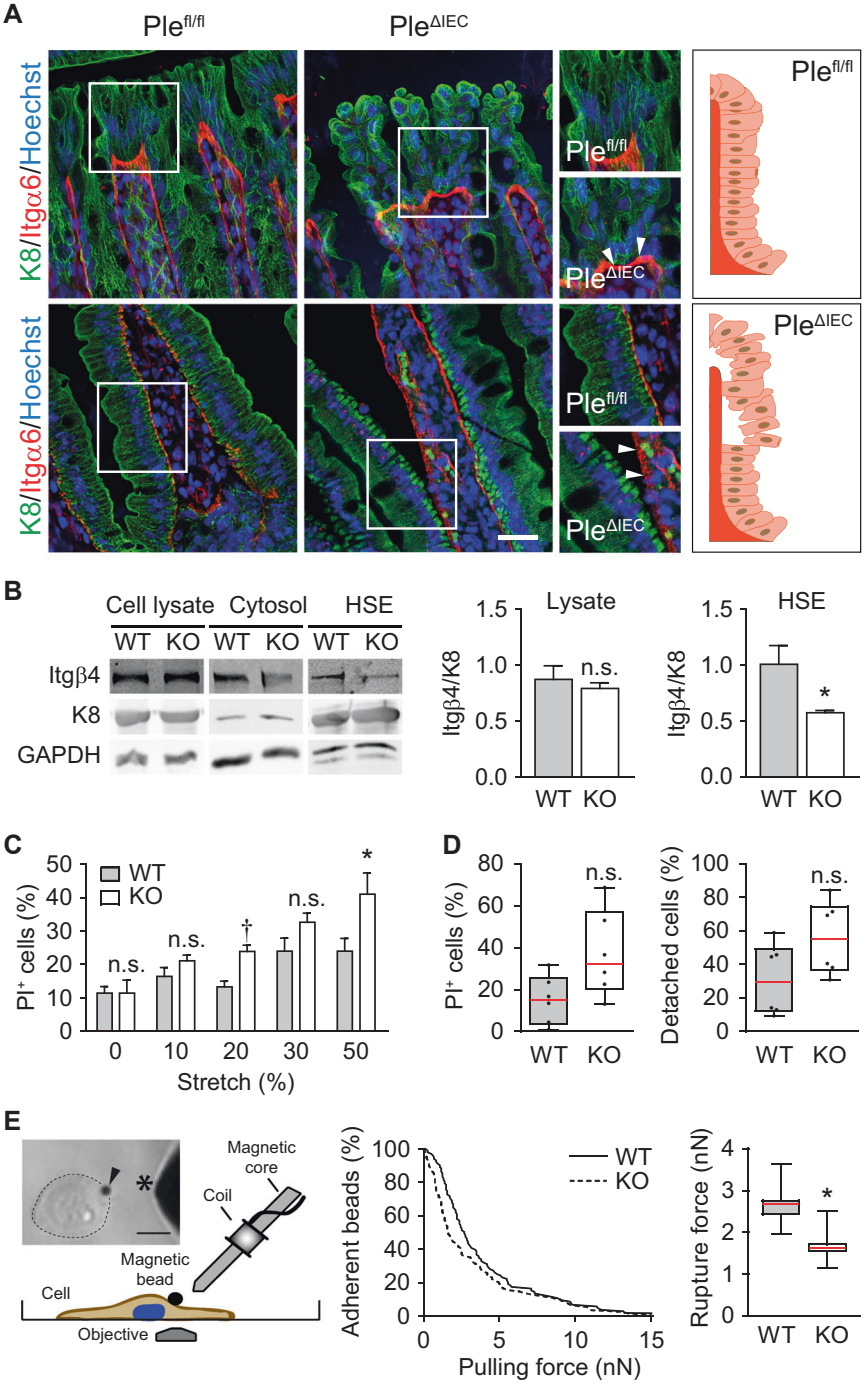

Fig. 5 Plectin stabilizes IEC hemidesmosomes through KF recruitment. A Representative immunofluorescence images of *Ple*$^{fl/fl}$ and *Ple*$^{\Delta IEC}$ distal colon (upper panels) and small intestine (lower panels) sections immunolabeled for K8 (green) and Itgα6 (red); Hoechst-stained nuclei (blue). Arrowheads, Itgα6-positive clusters. Scale bar, 25 µm. Boxed areas show ×1.5 images. Drawn schematics depict aligned, BM-attached *Ple*$^{fl/fl}$ IECs (upper panel) and mislocalized, detaching *Ple*$^{\Delta IEC}$ IECs (lower panel). **B** Cell lysates, cytosol fractions, and keratin-enriched high salt extracts (HSE) were prepared from WT and KO Caco-2 cells and subjected to immunoblotting with antibodies to Itgβ4 and K8. GAPDH, loading control. Graphs show relative band intensities normalized to average *Ple*$^{fl/fl}$ values, $n = 4$–6. **C** Viability of WT and KO Caco-2 cells exposed to uniaxial cyclic stretch presented as a percentage of dead (PI-positive; PI^+) cells, $n = 9$–11. **D** Quantification of WT and KO Caco-2 cell viability (left) and adhesion (right) under radial shear flow shown as a percentage of dead and detached cells, respectively, $n = 6$. Boxplot data represent median, 25th, and 75th percentile with whiskers reaching the last data point. **E** Adhesion strength between ECM-coated superparamagnetic beads and WT and KO Caco-2 cells was quantified using magnetic tweezers that generated forces ramps at a speed of 1 nN/s up to a maximum force of 15 nN. Image and schematic depict magnetic tweezer setup. Arrowhead, paramagnetic bead; asterisk, magnetic tweezer tip; dotted circular line, cell border. Scale bar, 20 µm. The graph shows the percentage of beads ($n = 103$ WT, 109 KO cells) that remained adherent at a given pulling force. The boxplot shows the distribution of the median detachment force (calculated from bootstrapping by sampling with replacement, $n = 1000$ runs) and its distribution (25th, and 75th percentile with whiskers reaching the minimum and maximum sampled values). Bar graph data in all other subplots represent mean ± SEM, n.s. not significant, $^*P < 0.05$, $^\dagger P < 0.001$.

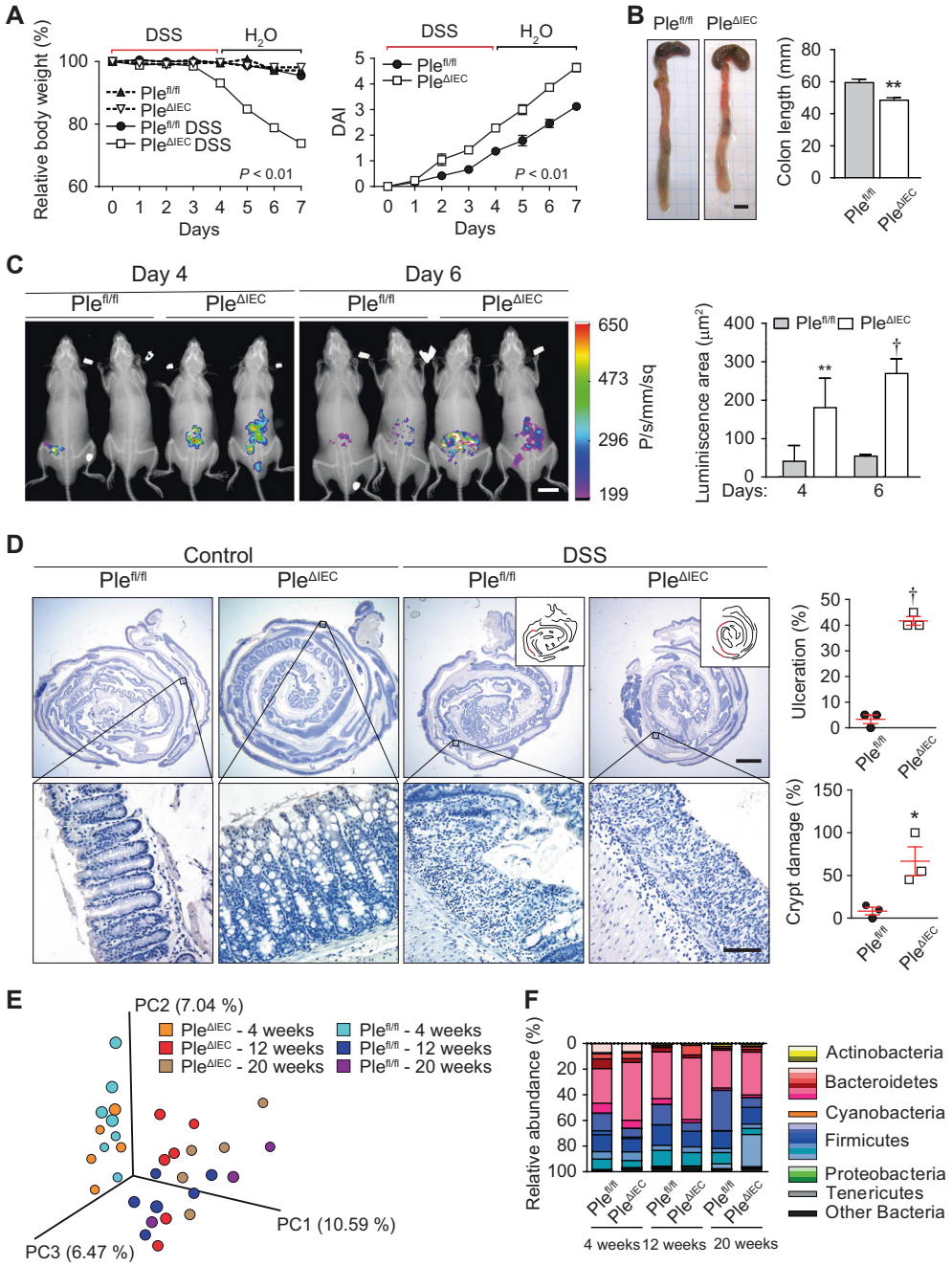

Fig. 6 ***Ple*$^{\Delta IEC}$ mice are more susceptible to DSS-induced colitis. A** Relative bodyweight and disease activity index (DAI) of untreated and DSS-treated *Ple*$^{fl/fl}$ and *Ple*$^{\Delta IEC}$ mice during experimental colitis. Four to seven mice per genotype and time point were analyzed. **B** Representative images of colon and caecum of DSS-treated *Ple*$^{fl/fl}$ and *Ple*$^{\Delta IEC}$ mice. The graph shows colon length, $n = 4$–6. **C** In vivo chemiluminescence images and signal quantification (graph) of DSS-treated *Ple*$^{fl/fl}$ and *Ple*$^{\Delta IEC}$ mice injected with the myeloperoxidase substrate luminol on days 4 and 6 of DSS treatment, $n = 3$–4. **D** Representative hematoxylin-stained sections of Swiss roll mounts from untreated (control) and DSS-treated (DSS) mice. Scale bars, 2 mm, magnified boxed areas, 100 µm. Insets, outlines of lesions (in red) distributed along mucosa (black lines) in corresponding panels. Graphs show quantification of colonic tissue damage given as the percentage of ulceration and crypt damage, $n = 3$, **E**, **F** Fecal microbiota beta diversity in 4-, 12-, and 20-week-old untreated *Ple*$^{fl/fl}$ and *Ple*$^{\Delta IEC}$ mice as determined by 16S rDNA sequencing. Principal coordinate analysis plot (**E**), constructed with unweighted UniFrac distance metric, shows clustering of microbial beta diversity. PC1, PC2, and PC3 represent the top three principal coordinates that captured most of the diversity (given as a percentage). Global composition (**F**) of bacterial microbiota at phyla level shown as relative operational taxonomic unit (OTUs) abundance per time point and genotype, $n = 4$–6. Data are presented as mean ± SEM, $^{*}P < 0.05$, $^{**}P < 0.01$, †$P < 0.001$.

To gain better control over *plectin* inactivation timing, we generated TMX-inducible IEC-specific *plectin* knockout (*Ple*$^{\Delta IEC\text{-}ERT2}$) mice. Three consecutive applications of TMX in 9-week-old *Ple*$^{\Delta IEC\text{-}ERT2}$ mice resulted in recombination efficiency comparable to that of constitutive *Ple*$^{\Delta IEC}$ mice, and a distinctive intestinal phenotype developed as early as 5 days post-TMX administration (not shown). To determine the effect of a diet change on the intestinal injury, *Ple*$^{\Delta IEC\text{-}ERT2}$ and *Ple*$^{fl/fl}$ control mice were either

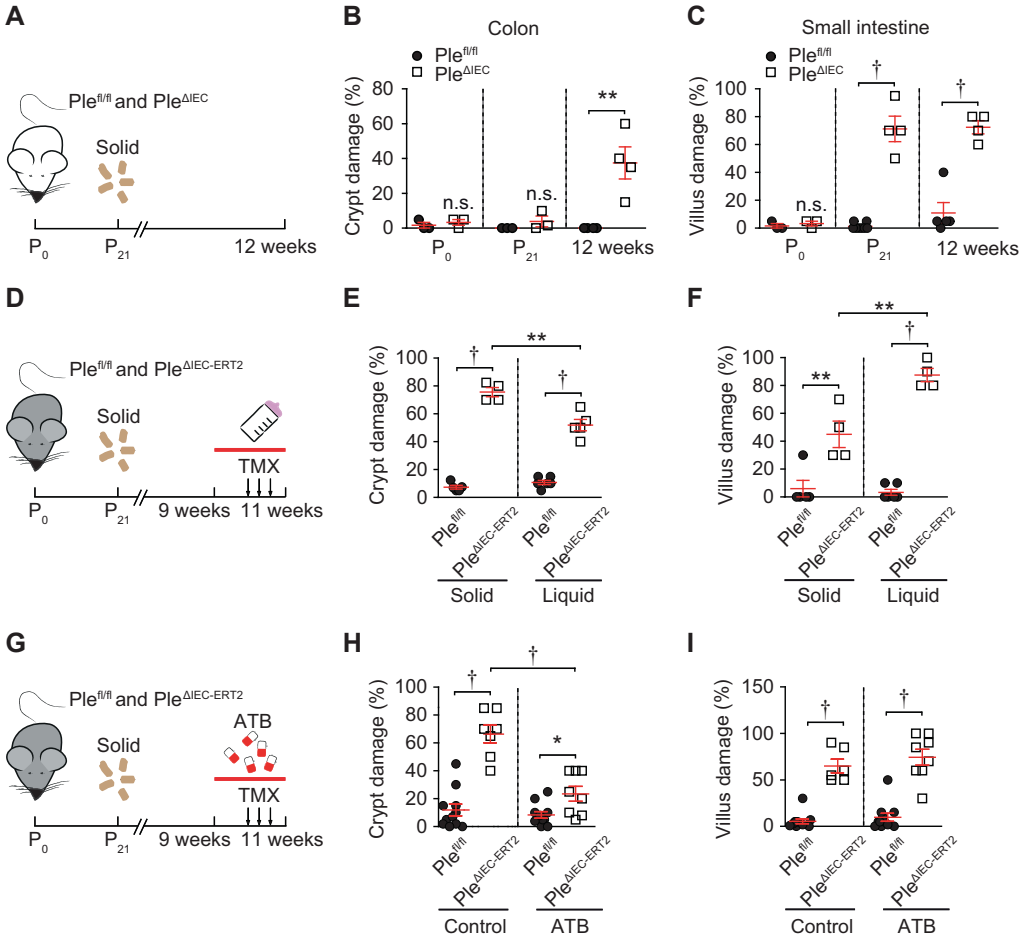

Fig. 7 Intestinal epithelial damage in *Ple*$^{\Delta IEC}$ mice results from mechanical stress. A–C *Ple*$^{fl/fl}$ and *Ple*$^{\Delta IEC}$ mice were sacrificed on postnatal day 0 (P0), postnatal day 21 (P21), and at 12 weeks (12w) of age, and epithelial damage scores were assessed from colon and small intestine sections. Schematic illustrates the experimental setup (**A**). Solid, transition to solid chow at P21. Graphs show quantification of epithelial damage in the colon (**B**) and small intestine (**C**) at the age indicated. **D–F** Nine-week-old *Ple*$^{fl/fl}$ and *Ple*$^{\Delta IEC- ERT2}$ mice were either kept on solid chow or provided with a liquid diet for 14 days. *Plectin* inactivation was induced by three consecutive applications of tamoxifen (TMX) on days 6, 8, and 10; mice were sacrificed on day 14. The schematic illustrates the experimental setup (**D**). Solid, transition to solid chow at P21; arrows, TMX application; red bar, period on a liquid diet. Graphs show quantification of epithelial damage in the colon (**E**) and small intestine (**F**) on solid chow and liquid diet. **G–I** Nine-week-old *Ple*$^{fl/fl}$ and *Ple*$^{\Delta IEC-ERT2}$ mice were kept either untreated or treated with broad-spectrum antibiotics. *Plectin* inactivation and sample collection were identical to (**B**). Schematics illustrate experimental setup (**G**). Chow, the transition to solid chow at P21; arrows, TMX application; red bar, period of antibiotics (ATB) treatment. Graphs show quantification of epithelial damage in the colon (**H**) and small intestine (**I**) on solid chow and liquid diet. Data are presented as mean ± SEM, n.s. not significant, **P* < 0.05, ***P* < 0.01, †*P* < 0.001.

kept on solid chow or provided with a low-residue liquid diet 6 days before TMX administration. The liquid diet significantly attenuated epithelial damage in the colon of *Ple*$^{\Delta IEC-ERT2}$ mice; however, the histological score indicates more severe injury of the small intestine (Figs. 7D–F and S11B). The beneficial effects of the liquid diet also manifested as less prominent colon swelling (not shown).

As previous studies linked the severity of colitis and intestinal injury with commensal microbiota[8,35], next we treated *Ple*$^{fl/fl}$ and *Ple*$^{\Delta IEC-ERT2}$ mice with well-established broad-spectrum antibiotics[8]. In our experimental setup, the apparent milder colitic phenotype consistently coincided with lower epithelial damage in the colon of *Ple*$^{\Delta IEC-ERT2}$ mice. This treatment however did not affect epithelial injury of the *Ple*$^{\Delta IEC-ERT2}$ small intestine (Figs. 7G–I and S11C). Collectively, these data support the notion that the increased susceptibility of the plectin-deficient intestinal epithelium to mechanical strain impinged by luminal content is caused by a lack of KF attachment to Itg clusters and destabilization of intestinal HDs. Further, the fact that antibiotics also partially alleviate epithelial damage suggests that luminal bacteria significantly contribute to intestinal injury in *Ple*$^{\Delta IEC-ERT2}$ mice.

DISCUSSION

The intestinal epithelium faces substantial mechanical stress[36], which is inextricably linked to gut physiology. Although several studies suggest the importance of intestinal KF networks[35,37,38] and KF-associated cell junctions (Ds and HDs)[8,9] for protection against intestinal inflammation and CRC, the contribution of altered epithelial mechanics to observed phenotypes remain unexplored. Here, we focus on the role of KF-cell junction linker plectin in the maintenance of intestinal homeostasis, and we provide a comprehensive analysis of molecular mechanisms governing the mechanical stability of intestinal epithelia.

The most notable phenotype of both plectin-deficient mouse models (*Ple*$^{\Delta IEC}$ and *Ple*$^{\Delta IEC-ERT2}$) is the detachment of IECs from the

underlying BM, resulting in extensive epithelial injury and eventually in the spontaneous development of a colitic phenotype. Strikingly, this is accompanied by loss of the hemidesmosomal ECM receptor Itgα6 from detached IECs, while Itgα6 patches remain on a collagen-stained BM, likely indicating their inefficient linkage to cytoskeletal structures. Indeed, our TEM analysis revealed that less electrodense HDs formed by $Ple^{\Delta IEC}$ IECs were somewhat elongated, and gaps between HD plaques and the BM were significantly wider compared to $Ple^{fl/fl}$ IECs. The formation of morphologically abnormal HDs was paralleled with reduced expression levels of both HD-forming integrins (α6 and β4) in the $Ple^{\Delta IEC}$ mucosa. Moreover, the content of Itgβ4 was also significantly diminished in keratin-enriched fractions prepared from plectin-deficient IECs, suggesting the reduced association of Itgα6β4 complexes with intestinal keratins (K8, 18, and 19).

Our observations are concordant with a recently published model for skin type I HD[10], which proposed that plectin (along with BPAG, another plakin family member) fortifies HD plaques both horizontally (by a lateral association of Itgβ4) and vertically (by interlinking Itgβ4 with KFs). Accordingly, ablation of plectin, the only plakin present in intestinal-type II HD[39], would fully abrogate a functional link between KFs and HDs and would result in their overall destabilization. In line with this hypothesis, we in vitro show a trend towards higher detachment (paralleled with a higher death rate) of plectin-deficient IECs exposed to a uniaxial cyclic stretch and a constant radial flow compared to their WT counterparts. As both $Ple^{fl/fl}$ and $Ple^{\Delta IEC}$ IECs display a minimal degree of spontaneous apoptosis in vivo, the observed excessive cell death in our experiments in vitro can likely be attributed to incomparable force magnitude and cell context under these two conditions. Consistent with our results from cell stretching and radial shear assays, we also determine significantly lower adhesion strength between ECM-coated superparamagnetic beads and plectin-deficient IECs using magnetic tweezers. Hence, by combining in vivo and in vitro approaches, we provide evidence that plectin is essential for the stability of intestinal HD type II, a structure preventing colitis[8] and presumably also the risk of colitis-associated CRC[8,40,41].

Previous studies demonstrated that the deletion of *plectin* has adverse effects on the formation of intercellular junctions, with consequences for the epithelial barrier function[21,22]. It has been shown that plectin-deficient cholangiocytes form dysfunctional Ds and fail to upregulate some desmosomal proteins, such as desmoplakin, a putative binding partner of plectin[42], in response to bile stasis[22]. This failure results in mechanical weakening of the biliary epithelium and contributes to plectin-related familial intrahepatic cholestasis[43]. In terms of mechanistic parallels between plectin-deficient biliary and intestinal epithelia, we found that apart from destabilizing HDs, plectin deficiency also leads to the prominent broadening of Ds, AJs, and TJs. Moreover, $Ple^{\Delta IEC}$ IECs exhibit downregulation of corresponding junctional constituents (ZO-1, E-cad, Dsg2, and Dsp1/2). Although the resulting dilatation of intercellular spaces would per se suffice to explain the observed increase in intestinal permeability and bacterial penetration, the "leaky gut" in $Ple^{\Delta IEC}$ mice seems ultimately rooted in the less firm IEC/BM connection, given the extent of IEC detachment. On the other hand, proper anchorage of KFs (determining cell mechanics) to Ds (ensuring intercellular cohesion) is known to provide load-bearing tissues with mechanical stability[11]. Showing altered KF cytoarchitecture and aberrant D formation in both in vitro plectin-deficient IEC systems and $Ple^{\Delta IEC}$ mice, our results suggest that D-keratin complex abnormality substantially contributes to the compromised mechanics of the $Ple^{\Delta IEC}$ intestinal epithelium.

We propose that the lack of functional plectin at HDs (in combination with its effects on KFs and Ds) and the resulting mechanical epithelial fragility favor an impaired intestinal barrier function and are ultimately responsible for colitis. Importantly, comparable mucosal deterioration was observed upon plectin ablation during development and in the adult intestine with its fully mature immune system. Furthermore, we also demonstrate that loss of plectin can exacerbate experimental colitis in mice. Consistent with these results, lower expression levels of plectin correlate with UC development in human patients, suggesting that defects in cytoskeleton coordination mediated through plectin contribute to IBD pathogenesis in humans by affecting IEC/BM adhesion, IEC cohesion, and mechanical properties. However, it is well recognized that properly organized KF networks[38,44], HDs[8], and intercellular junctions[2,3,9] exert numerous non-mechanical functions, providing the intestinal epithelium with protection against microbial infection and uncontrolled inflammation. Our data do not rule out similar functions in the $Ple^{\Delta IEC}$ intestine. Further studies will be required to investigate how plectin deficiency affects cell-autonomous (barrier function-independent) mechanisms involved in the interplay between IECs, gut microbiota, and immune cells.

We observed a prominent hyperproliferation of plectin-deficient IECs paralleled by a dramatically higher proportion of PAS-positive goblet cells. This phenotype closely resembles the situation in mice lacking hemidesmosomal α6 integrin[8] or K8[45,46]. Together, these findings suggest that the keratin/plectin/integrin axis is essential for balanced proliferation and differentiation of IECs. Interestingly, intestinal K8 and K18 were shown to promote Notch1 signaling, a major pathway of colonic cell fate specification[46]. Since Notch-mediated signal transduction depends on cytoskeletal tension[47,48], it is tempting to speculate that intact plectin-controlled KF cytoarchitecture facilitates mechano-regulation of intestinal cell fate. Moreover, plectin anchors the cytoskeleton to the nuclear envelope via interaction with nesprin-3[49] and mediates transmission of mechanical stimuli directly to the nucleus. Multiple studies provide evidence that loss of plectin results in nuclear phenotypes, including altered nuclear positioning[22], nuclear deformations[50,51], chromatin modification, and gene expression[51]. To elucidate whether and how plectin regulates specific transcriptional programs in IECs and to find their contribution to the proper spatiotemporal proliferation/differentiation pattern within colonic crypts is a goal of our ongoing studies.

The rapid deterioration of the $Ple^{\Delta IEC}$ intestinal mucosa following weaning (i.e., a switch to a solid diet and the amplification of muscle contractions) indicates that the origin of colitis in the absence of plectin is primarily associated with a reduced capacity of IECs to resist mechanical stress. In addition, the most severe epithelial injury was found in the distal colon, which is the region most intensely subjected to such stress. Comparably devastating epithelial instability has been well documented for epidermal layers in EB patients[15,16]. As there is no causal therapy for EB available[15], the current treatment focuses mainly on the prevention of tissue destruction. Following the same rationale, we demonstrate that a low-residue liquid diet significantly attenuates colonic epithelial damage, thus protecting its barrier function. Surprisingly, this approach aggravates IEC detachment in the $Ple^{\Delta IEC}$ small intestine, which might suggest augmented susceptibility of the small intestine to plectin loss. Therefore, future studies should investigate whether differential expression of plectin along the gastrointestinal tract might have an impact on regional differences in disease manifestations in patients. In line with the previous observations[8,35], antibiotic treatments markedly decrease not only mucosal inflammation but, intriguingly, also epithelial damage, which implies that host-microbiota interactions contribute to excessive IEC sloughing in the $Ple^{\Delta IEC}$ intestine. Although dietary factors can likely ameliorate only less extensive trauma, our results suggest that a low-residue liquid diet combined with antibiotic treatment might be a useful palliative modality. To translate our findings into clinical

medicine: it remains to be determined whether such a strategy (i) is suitable for long-term treatment and (ii) is effective with respect to systemic disease manifestation.

METHODS

Patients

Colon biopsy samples were collected from patients diagnosed with UC ($n = 97$) and from healthy controls ($n = 20$) admitted to the Hepatogastroenterology Department at the Institute for Clinical and Experimental Medicine (Prague, Czech Republic) for a colonoscopy from July 2016 to May 2019. Subjects were assigned to the healthy control group only after all clinical examinations excluded any signs of autoimmune disease, inflammatory disease, and colon cancer. All UC patients with concurrent primary sclerosing cholangitis (PSC) were excluded from the study. Endoscopic UC activity at the time of a standard optical colonoscopy was categorized according to the Mayo endoscopic subscore and confirmed by histology examinations of the grade of inflammation. Clinical characteristics of patients are shown in Supplementary Table S1. Standard endoscopic biopsies were extracted from the inflamed non-dysplastic mucosa of the left colon (rectum) and immediately placed in an RNAlater solution. Total RNA was extracted according to the manufacturer's instructions.

Mice

Plectin$^{flox/flox}$ (*Ple*$^{fl/fl}$) mice[23] were crossed with *villin-Cre* transgenic mice (MGI 2448639) to generate *Ple*$^{fl/fl}$*/villin-Cre* mice (*Ple*$^{\Delta IEC}$) and with *villin-creERT2* transgenic mice (MGI 3053826; both Cre strains were kindly provided by S. Robine[52]) to generate *Ple*$^{fl/fl}$*/villin-creERT2* mice (*Ple*$^{\Delta IEC\text{-}ERT2}$). Age-matched littermate male mice were used in all experiments. Unless stated otherwise, mice were 12–14 weeks old. Animals were housed under specific pathogen-free conditions with regular access to chow and drinking water and a 12 h light/12 h dark regime.

Cells and CRISPR-mediated targeting of plectin

Caco-2 cells were grown in Dulbecco's modified Eagle medium (DMEM) supplemented with 20% fetal bovine serum (FBS) in a 5% CO_2/air humidified atmosphere at 37 °C. Human colonic cells (hCC; T0570, Applied biological materials, Inc.) were cultured in DMEM supplemented with 10% FBS in 5% CO_2/air humidified atmosphere at 37 °C. Plectin knockout (KO) cell lines were generated by targeting genomic sequences of intron 25–26 and exon 31 of *Plectin* using CRISPR/Cas9 plasmid pX330 Cas9-Venus (a kind gift of B. Schuster, IMG CAS, Prague, Czech Republic) as described previously[22]. The potential off-target sites were predicted using CRISPOR (http://crispor.tefor.net/). The four top-ranking potential off-target sites for each guide RNA were selected for validation. The genomic DNA sequences surrounding the potential off-target sites were amplified by PCR using gene-specific primers (Supplementary Table 3). PCR products were analyzed by direct sequencing (Figs. S12 and S13).

Statistics

All results are presented as mean ± SEM. All normally distributed parametric data were analyzed by two-tailed unpaired Student *t* test. Comparisons of multiple groups to controls were performed using two-tailed one-way ANOVA. Comparisons of frequency distributions of BrdU-positive cells were analyzed with Mann–Whitney test. Survival curves were analyzed by Mantel–Cox test. Statistical analyses were performed using GraphPad Prism 5 (GraphPad Software, Inc., La Jolla, CA). Comparisons of detachment forces were done with bootstrapping (sampling with replacement) with 1000 replicates. Statistical significance was determined at the levels of $^{*}P < 0.05$, $^{**}P < 0.01$, $^{\dagger}P < 0.001$; n values are specified in the figure legends.

Study approval

This study was approved by the Ethics Committee of the Institute for Clinical and Experimental Medicine and Thomayer Hospital with Multi-Center Competence (G16-06-25). Written informed consent was obtained from all subjects before the study. All animal studies were performed in accordance with European Directive 2010/63/EU and were approved by the Czech Central Commission for Animal Welfare (48/2014 and 23/2020).

ACKNOWLEDGEMENTS

We would like to thank L. Macurek (IMG CAS, Prague) for generously providing the hCC cell line, S. Robine (Institut Curie, Paris) for Cre mouse lines, and B.Schuster (IMG CAS, Prague) for pX330 Cas9-Venus plasmid; H. Havelkova (IMG CAS, Prague) and I. Muricova (Institute of Physiology CAS, Prague) for their outstanding technical assistance; S. Reipert (University of Vienna, Vienna), M. Efenbergova, J. Tureckova (both IMG CAS, Prague), and Z. Jiraskova (Institute of Microbiology CAS, Prague) for their expertize; and T. Epp, M. Prechova (both IMG CAS, Prague) and A.I. Ivanov (Lerner Research Institute of Cleveland Clinic Foundation, Cleveland) for critical reading of the manuscript. We acknowledge the Light and Electron Microscopy Core Facilities, IMG CAS, Prague, Czech Republic, for their support with advanced microscopy imaging.

AUTHOR CONTRIBUTIONS

Study concept and design: M.G.; acquisition of data: A.K., P.B., L.S., G.O.-E., G.K., J. Prochazka, M.S., C.D., Z.S., M.V., N.Z.; analysis and interpretation of data: A.K., M.G., J.S., E.S., L.B., J. Pacha, J. Prochazka, D.J., M.K., B.F.; drafting of the manuscript: A.K, M.G.; critical revision of the manuscript for important intellectual content: all authors. Funding: M.G., M.K., G.W., B.F. technical and material support: P.W., L.B., V.K., R.S., G.W.

FUNDING

This work was supported by the Grant Agency of the Ministry of Health of the Czech Republic (17-31538A); the Czech Academy of Sciences (L200521601; postdoctoral fellowship to AK); the Grant Agency of the Czech Republic (17-09869S and 20-16520Y); the Institutional Research Project of the Czech Academy of Sciences (RVO 68378050); COST Action CA15214-EuroCellNet, Strategy AV21—QUALITAS; the Grant Agency of Charles University (192119); TACR GAMA 2 (TP01010031); MH CZ—DRO (Institute for Clinical and Experimental Medicine—IKEM, IN 00023001); MEYS CR projects (LQ1604 NPU II, LTC17063, LM2015062, LO1419, and LM2015040); MEYS CR/ERDF projects (OP RDI CZ.1.05/2.1.00/19.0395 and CZ.1.05/1.1.00/02.0109); MEYS CR/ESIF project OP RDE CZ.02.1.01/0.0/0.0/16_013/0001775; the Operational Program Prague–Competitiveness project (CZ.2.16/3.1.00/21547); the German Science Foundation (DFG FA 336/12-1); and the Austrian Science Research Fund (FWF grant I413-B09).

ADDITIONAL INFORMATION

Supplementary information The online version contains supplementary material available at https://doi.org/10.1038/s41385-021-00380-z.

Competing interests: The authors declare no competing interests.

Publisher's note Springer Nature remains neutral with regard to jurisdictional claims in published maps and institutional affiliations.

REFERENCES

1. Camilleri M. Leaky gut: mechanisms, measurement and clinical implications in humans. *Gut*. **68**, 1516–1526 (2019).
2. Pastorelli, L., De Salvo, C., Mercado, J. R., Vecchi, M. & Pizarro, T. T. Central role of the gut epithelial barrier in the pathogenesis of chronic intestinal inflammation: lessons learned from animal models and human genetics. *Front. Immunol.* **4**, 1–22 (2013).
3. Peterson, L. W. & Artis, D. Intestinal epithelial cells: regulators of barrier function and immune homeostasis. *Nat. Rev. Immunol.* **14**, 141–153 (2014).
4. Consortium, U. I. G. et al. Genome-wide association study of ulcerative colitis identifies three new susceptibility loci, including the HNF4A region. *Nat. Genet.* **41**, 1330–1334 (2009).
5. McGovern, D. P. et al. Genome-wide association identifies multiple ulcerative colitis susceptibility loci. *Nat. Genet.* **42**, 332–337 (2010).

6. Anderson, C. A. et al. Meta-analysis identifies 29 additional ulcerative colitis risk loci, increasing the number of confirmed associations to 47. *Nat. Genet.* **43**, 246–252 (2011).
7. Garcia, M. A., Nelson, W. J. & Chavez, N. Cell–cell junctions organize structural and signaling networks. *Cold Spring Harb. Perspect. Biol.* **10**, 1–27 (2018).
8. De Arcangelis, A. et al. Hemidesmosome integrity protects the colon against colitis and colorectal cancer. *Gut* **66**, 1748–1760 (2017).
9. Gross, A. et al. Desmoglein 2, but not desmocollin 2, protects intestinal epithelia from injury. *Mucosal Immunol.* **11**, 1630–1639 (2018).
10. Walko, G., Castanon, M. J. & Wiche, G. Molecular architecture and function of the hemidesmosome. *Cell Tissue Res.* **360**, 529–544 (2015).
11. Hatzfeld, M., Keil, R. & Magin T. M. Desmosomes and intermediate filaments: their consequences for tissue mechanics. *Cold Spring Harb. Perspect. Biol.* **9**, 1–20 (2017).
12. Ruhrberg, C. & Watt, F. M. The plakin family: versatile organizers of cytoskeletal architecture. *Curr. Opin. Genet. Dev.* **7**, 392–397 (1997).
13. Wiche, G., Osmanagic-Myers, S. & Castanon, M. J. Networking and anchoring through plectin: a key to IF functionality and mechanotransduction. *Curr. Opin. Cell Biol.* **32**, 21–29 (2015).
14. Rezniczek, G. A., Walko, G. & Wiche, G. Plectin gene defects lead to various forms of epidermolysis bullosa simplex. *Dermatol. Clin.* **28**, 33–41 (2010).
15. Uitto, J., Bruckner-Tuderman, L., McGrath, J. A., Riedl, R. & Robinson, C. EB2017-progress in epidermolysis bullosa research toward treatment and cure. *J. Investig. Dermatol.* **138**, 1010–1016 (2018).
16. Has, C. & Fischer, J. Inherited epidermolysis bullosa: new diagnostics and new clinical phenotypes. *Exp. Dermatol.* **28**, 1146–1152 (2018).
17. Smith, P. K. et al. Epidermolysis bullosa and severe ulcerative colitis in an infant. *J. Pediatr.* **122**, 600–603 (1993).
18. Freeman, E. B. et al. Gastrointestinal complications of epidermolysis bullosa in children. *Br. J. Dermatol.* **158**, 1308–1314 (2008).
19. Osmanagic-Myers, S. et al. Plectin-controlled keratin cytoarchitecture affects MAP kinases involved in cellular stress response and migration. *J. Cell Biol.* **174**, 557–568 (2006).
20. Walko, G. et al. Targeted proteolysis of plectin isoform 1a accounts for hemidesmosome dysfunction in mice mimicking the dominant skin blistering disease EBS-Ogna. *PLoS Genet.* **7**, e1002396 (2011).
21. Osmanagic-Myers, S. et al. Plectin reinforces vascular integrity by mediating crosstalk between the vimentin and the actin networks. *J. Cell Sci.* **128**, 4138–4150 (2015).
22. Jirouskova, M. et al. Plectin controls biliary tree architecture and stability in cholestasis. *J. Hepatol.* **68**, 1006–1017 (2018).
23. Ackerl, R. et al. Conditional targeting of plectin in prenatal and adult mouse stratified epithelia causes keratinocyte fragility and lesional epidermal barrier defects. *J. Cell Sci.* **120**, 2435–2443 (2007).
24. Huang, B. L., Chandra, S. & Shih, D. Q. Skin manifestations of inflammatory bowel disease. *Front. Physiol.* **3**, 13 (2012).
25. Wiche, G., Krepler, R., Artlieb, U., Pytela, R. & Denk, H. Occurrence and immunolocalization of plectin in tissues. *J. Cell Biol.* **97**, 887–901 (1983).
26. Kiesslich, R. et al. Local barrier dysfunction identified by confocal laser endomicroscopy predicts relapse in inflammatory bowel disease. *Gut* **61**, 1146–1153 (2012).
27. Chang, J. et al. Impaired intestinal permeability contributes to ongoing bowel symptoms in patients with inflammatory bowel disease and mucosal healing. *Gastroenterology* **153**, 723–731 e721 (2017).
28. Brauer, R. et al. MMP-19 deficiency causes aggravation of colitis due to defects in innate immune cell function. *Mucosal Immunol.* **9**, 974–985 (2015).
29. Luissint, A. C., Parkos, C. A. & Nusrat, A. Inflammation and the intestinal barrier: leukocyte-epithelial cell interactions, cell junction remodeling, and mucosal repair. *Gastroenterology* **151**, 616–632 (2016).
30. Gregor, M. et al. Mechanosensing through focal adhesion-anchored intermediate filaments. *FASEB J.* **28**, 715–729 (2014).
31. Kostan, J., Gregor, M., Walko, G. & Wiche, G. Plectin isoform-dependent regulation of keratin-integrin {alpha}6{beta}4 anchorage via Ca2+/calmodulin. *J. Biol. Chem.* **284**, 18525–18536 (2009).
32. Sartor, R. B. Mechanisms of disease: pathogenesis of Crohn's disease and ulcerative colitis. *Nat. Clin. Pr. Gastroenterol. Hepatol.* **3**, 390–407 (2006).
33. Pascal, V. et al. A microbial signature for Crohn's disease. *Gut* **66**, 813–822 (2017).
34. Bajer, L. et al. Distinct gut microbiota profiles in patients with primary sclerosing cholangitis and ulcerative colitis. *World J. Gastroenterol.* **23**, 4548–4558 (2017).
35. Habtezion, A. et al. Absence of keratin 8 confers a paradoxical microflora-dependent resistance to apoptosis in the colon. *Proc. Natl. Acad. Sci. USA* **108**, 1445–1450 (2011).
36. Gayer, C. P. & Basson, M. D. The effects of mechanical forces on intestinal physiology and pathology. *Cell Signal.* **21**, 1237–1244 (2009).
37. Baribault, H., Penner, J., Iozzo, R. V. & Wilson-Heiner, M. Colorectal hyperplasia and inflammation in keratin 8-deficient FVB/N mice. *Genes Dev.* **8**, 2964–2973 (1994).
38. Habtezion, A., Toivola, D. M., Butcher, E. C. & Omary, M. B. Keratin-8-deficient mice develop chronic spontaneous Th2 colitis amenable to antibiotic treatment. *J. Cell Sci.* **118**, 1971–1980 (2005).
39. Litjens, S. H., de Pereda, J. M. & Sonnenberg, A. Current insights into the formation and breakdown of hemidesmosomes. *Trends Cell Biol.* **16**, 376–383 (2006).
40. Beaulieu, J. F. Integrin I+/-6 variants and colorectal cancer. *Gut* **67**, 1747–1748 (2018).
41. De Arcangelis, A., Chamaillard, M., Simon-Assmann, P. & Labouesse, M. Integrin a6 loss promotes colitis-associated colorectal cancer. Response to: "Integrin a6 variants and colorectal cancer" by Beaulieu JF. *Gut* **67**, 2227–2228 (2018).
42. Eger, A., Stockinger, A., Wiche, G. & Foisner, R. Polarisation-dependent association of plectin with desmoplakin and the lateral submembrane skeleton in MDCK cells. *J. Cell Sci.* **110**, 1307–1316 (1997).
43. Wu, S. H. et al. Plectin mutations in progressive familial intrahepatic cholestasis. *Hepatology* **70**, 2221–2224 (2019).
44. Geisler, F. & Leube, R. E. Epithelial intermediate filaments: guardians against microbial infection? *Cells*. **5**, 1–18 (2016).
45. Toivola, D. M., Krishnan, S., Binder, H. J., Singh, S. K. & Omary, M. B. Keratins modulate colonocyte electrolyte transport via protein mistargeting. *J. Cell Biol.* **164**, 911–921 (2004).
46. Lahdeniemi, I. A. K. et al. Keratins regulate colonic epithelial cell differentiation through the Notch1 signalling pathway. *Cell Death Differ.* **24**, 984–996 (2017).
47. Luca, V. C. et al. Notch-Jagged complex structure implicates a catch bond in tuning ligand sensitivity. *Science* **355**, 1320–1324 (2017).
48. Hunter, G. L. et al. A role for actomyosin contractility in Notch signaling. *BMC Biol.* **17**, 12 (2019).
49. Ketema, M., Kreft, M., Secades, P., Janssen, H. & Sonnenberg, A. Nesprin-3 connects plectin and vimentin to the nuclear envelope of Sertoli cells but is not required for Sertoli cell function in spermatogenesis. *Mol. Biol. Cell* **24**, 2454–2466 (2013).
50. Almeida, F. V. et al. The cytolinker plectin regulates nuclear mechanotransduction in keratinocytes. *J. Cell Sci.* **128**, 4475–4486 (2015).
51. Staszewska, I., Fischer, I. & Wiche, G. Plectin isoform 1-dependent nuclear docking of desmin networks affects myonuclear architecture and expression of mechanotransducers. *Hum. Mol. Genet.* **24**, 7373–7389 (2015).
52. el Marjou, F. et al. Tissue-specific and inducible cre-mediated recombination in the gut epithelium. *Genesis* **39**, 186–193 (2004).

Limited Validity of Mayo Endoscopic Subscore in Ulcerative Colitis with Concomitant Primary Sclerosing Cholangitis

Pavel Wohl[1]†, Alzbeta Krausova[2], Petr Wohl[3], Ondrej Fabian[4,5], Lukas Bajer[1], Jan Brezina[1], Pavel Drastich[1], Mojmír Hlavaty[1], Petra Novotna[2], Michal Kahle[6], Julius Spicak[1], Martin Gregor[2*]

[1]Department of Gastroenterology, Institute for Clinical and Experimental Medicine, Prague, Czech Republic

[2]Laboratory of Integrative Biology, Institute of Molecular Genetics of the Czech Academy of Sciences, Prague, Czech Republic

[3]Diabetes Center, Institute for Clinical and Experimental Medicine, Prague, Czech Republic

[4]Department of Clinical and Transplant Pathology, Institute for Clinical and Experimental Medicine, Prague, Czech Republic

[5]Department of Pathology and Molecular Medicine, 3rd Faculty of Medicine, Charles University and Thomayer Hospital, Prague, Czech Republic

[6]Department of Data Analysis, Statistics, and AI, Institute for Clinical and Experimental Medicine, Prague, Czech Republic

Short title: Mayo Endoscopic Subscore in PSC-UC patients

*Corresponding author: Martin Gregor, E-mail: martin.gregor@img.cas.cz

†Co-corresponding author: pavel.wohl@ikem.cz

Word count (main body): 2,447

Number of Figures: 3

Number of Tables: 2

Data Availability

The data underlying this article cannot be shared publicly due to the privacy of individuals that participated in this study. The data will be shared on reasonable request to the corresponding authors.

Funding

This work was supported by the Grant Agency of the Ministry of Health of the Czech Republic [NV17-31538A to M.G. and Pa.W.], the Grant Agency of the Czech Republic [20-16520Y to A.K. and 21-21736S to M.G.], and the Ministry of Education, Youth and Sports of the Czech Republic project NICR EXCELES [LX22NPO05102 to M.G.].

Conflict of Interest

The authors declare that there are no conflicts of interest to disclose.

Ethics approval

This study was approved by the Ethics Committee of the Institute for Clinical and Experimental Medicine and Thomayer Hospital with Multi-Center Competence (G16-06-25) and performed in accordance with the Declaration of Helsinki.

Patient Consent

Written informed consent was obtained from all patients.

Abstract

Background and Aims: Ulcerative colitis (UC) with concomitant primary sclerosing cholangitis (PSC) represents a distinct disease entity (PSC-UC). Mayo endoscopic subscore (MES) is a standard tool for assessing disease activity in UC but its relevance in PSC-UC remains unclear. Here, we sought to compare MES in a cohort of UC and PSC-UC patients and assess the accuracy using histological activity scoring (Nancy histological index; NHI).

Methods: MES was assessed in 30 PSC-UC and 29 UC adult patients during endoscopy. NHI and inflammation were evaluated in biopsies from the caecum, rectum, and terminal ileum. In addition, perinuclear anti-neutrophil cytoplasmic antibodies, fecal calprotectin, body mass index, and other relevant clinical characteristics were collected.

Results: The median MES and NHI were similar for UC patients (MES grade 2 and NHI grade 2 in the rectum), but were different for PSC-UC patients (MES grade 0 and NHI grade 2 in the caecum). There was a correlation between MES and NHI for UC patients (Spearman's $\rho = 0.40$, $p = 0.029$), but not for PSC-UC patients. Histopathological examination revealed persistent microscopic inflammation in 88% of PSC-UC patients with MES grade 0 (46% of all PSC-UC patients). Moreover, MES overestimated the severity of active inflammation in another 11% of PSC-UC patients.

Conclusion: MES fails to identify microscopic signs of inflammation in the context of PSC-UC. This indicates that histological evaluation should become an integral part of the diagnostic and grading system in both PSC-UC and PSC.

Key Words: Primary sclerosing cholangitis with ulcerative colitis; diagnosis; Nancy histological index; Mayo endoscopic subscore

1. Introduction

Primary sclerosing cholangitis (PSC) is a chronic cholestatic liver disease characterized by progressive inflammation, fibrosis, and diffuse multiple stricturing of the intrahepatic and extrahepatic bile ducts[1]. In up to 80% of patients, PSC is closely associated with inflammatory bowel disease (IBD), prevalently with a unique type of ulcerative colitis (UC) known as PSC-UC[2, 3].

As a distinct clinical phenotype, PSC-UC manifests with colonoscopic features that differ from those of typical UC without hepatobiliary disease. Interestingly, PSC-UC may not develop clinically apparent gastrointestinal symptoms[4, 5]. Multiple studies[2, 6, 7] have shown that the colonic inflammation in PSC-UC is typically more pronounced in the right-sided colon with often minimal to normal mucosal findings in the rectum. Furthermore, PSC-UC is characterized by a lower incidence of inflammatory polyps[4, 8] and a higher incidence of backwash ileitis[9] when compared to UC. In up to 94% of PSC-UC cases, the phenotype is reported as pancolitis with rectal sparing. Although colitis in PSC tends to follow a quiescent course, PSC-UC is associated with a high incidence of malignancies represented mainly by colitis-associated carcinoma (CAC)[10-13]. The risk of CAC is higher in PSC-UC than in UC alone, which is why accurate diagnosis is important for all PSC-UC patients.

IBD diagnosis is largely based on clinical symptoms, endoscopy, and histopathology[14] with endoscopic assessment being the most feasible and reliable approach[15] in routine clinical practice. Among many different endoscopic scores for UC[16], the Mayo Endoscopic Subscore (MES)[17, 18], a component of the Mayo Clinic Score, is recommended to assess disease activity and remains the most frequently used score in both clinical practice and clinical trials[17]. Surprisingly, despite accumulated evidence of limited diagnostic accuracy of endoscopic

techniques[19-23], namely in the context of mild mucosal inflammation, neither MES nor any of the other endoscopic scores have been validated for PSC-UC.

Endoscopy based approaches are not sufficiently reliable for PSC-UC patients. This can lead to poor therapeutic decisions and misguided treatment. Histopathological evaluation can remedy this by detecting potential microscopic disease activity, despite the absence of clinical or endoscopic signs of disease common in PSC-UC patients[19-23]. Out of the more than 30 described UC histological scores[24], the newly established Nancy Histological Index (NHI)[24-26], has quickly become one of the most popular histological scoring systems of inflammatory activity in UC. In 2020, the European Crohn's and Colitis Organization recommended NHI for daily clinical practice[27].

Given challenges of endoscopy for PSC-UC, the diagnostic relevance of MES for PSC-UC is unclear, despite MES being a standard tool for assessing inflammation in UC. The overall objective of this study was 1) to compare the reliability of MES as a diagnostic tool between UC and PSC-UC patient cohorts and 2) to assess the accuracy of MES in PSC-UC patients using histological disease activity scoring (NHI).

2. Methods

2.1 Patients

This study was a prospective longitudinal performed at the Institute for Clinical and Experimental Medicine (Prague, Czech Republic), a tertiary health care center. We included 59 Caucasian adult patients diagnosed with UC (n=29) and PSC-UC (n=30) according to conventional diagnostic criteria, who were admitted to the Hepatogastroenterology Department for a colonoscopy from July 2016 to March 2021. As portal hypertension with portal colopathy in liver cirrhosis are common endoscopic features that may mimic some inflammatory changes typical for PSC-UC, patients with advanced liver cirrhosis with portal hypertension were excluded. Other exclusion criteria were colitis-associated cancer and colonic dysplasia. Study cohort consisted of 20 females and 39 males (sex). This study was approved by the Ethics Committee of the Institute for Clinical and Experimental Medicine and Thomayer Hospital with Multi-Center Competence (G16-06-25) and performed in accordance with the Declaration of Helsinki. Written informed consents were obtained from all subjects before the study. All patients have been characterized as summarized in Table 1.

2.2 Endoscopic and histological evaluations

All UC and PSC-UC patients were subjected to a colonoscopy with a standard white light endoscope. During the colonoscopy, two or three biopsies from the terminal ileum, caecum, and rectum of endoscopically most severely inflamed mucosa were collected. Endoscopic disease activity was assessed using MES[17]. Histological inflammation in the colon biopsies (caecum and rectum) was assessed by NHI as published previously for UC[25,26]. In addition, histological inflammation in biopsies from the terminal ileum was determined by a four-grade scoring system (0-3), where 0 corresponds to normal and 3 to severe inflammation. Blinded

histopathological evaluation of paraffin-embedded sections stained with hematoxylin-eosin was performed by a trained pathologist (O.F.).

2.3 Primary sclerosing cholangitis

PSC was defined by the presence of intra- and/or extra-hepatic bile duct abnormalities in the form of beading, duct ectasia, and stricturing of the intra- or extra-hepatic bile ducts documented in the medical record from endoscopic retrograde cholangiopancreatography, magnetic resonance cholangiopancreatography, and/or liver biopsy. Small duct PSC was defined when there were histological features consistent with PSC on liver biopsy in the absence of characteristic radiological features. The diagnosis of PSC was also confirmed by laboratory tests (see below).

2.4 Laboratory and biochemical parameters

Blood analysis was performed on the day of the colonoscopy, including the determination of haemoglobin, leucocytes, platelets, and albumin (not shown). A stool sample that was obtained immediately before bowel preparation was provided by each patient for the analysis of faecal calprotectin (FC). FC level was measured by ELISA EliA kit (Phadia AB, Uppsala, Sweden). Detection of anti-neutrophil cytoplasmic antibody (ANCA) and IgG4 was performed using kits from Inova Diagnostics Inc., San Diego, USA.

2.5 Statistical analyses

All ordinal variables are presented as medians with 95% confidence intervals; continuous variables are expressed as means ± SEM. All differences between independent ordinal variables were tested by Mann-Whitney U test, differences in paired measurements were assessed by Wilcoxon signed-rank test and differences in proportions were tested by Fisher exact test.

Correlations are expressed as Spearman's rank correlation coefficient (ρ). For comparison of MES with NHI, only the most severely affected lesion with the highest NHI grade was considered for each patient. All data were analyzed using the Python ecosystem. Statistical significance was accepted at $p \leq 0.05$.

3. Results

3.1 MES and NHI scoring

The severity of UC was assessed both endoscopically and histologically in PSC-UC (Figure 1, upper panels) and UC (Figure 1, lower panels) patients. Endoscopy and histopathology involved examination of samples from the caecum, rectum and ileum. Among UC patients, only 2 individuals (7%) showed normal endoscopic findings (MES grade 0); the majority exhibited mild to moderate mucosal inflammation and damage (MES grades 1 and 2; median MES grade 2; Table 2). Similarly, histopathological examination revealed that most UC patients (90%) showed normal findings or mild inflammation with median NHI grade 1 in caecum (Table 2). However, in the rectum, 30% UC patients exhibited a shift towards moderately to severely active inflammation (median NHI grade 2; Table 2), which aligned with the MES findings. When considering the most severely inflamed biopsy for each patient (Figure 1, "caecum and rectum" panel), a significant correlation between MES and NHI was observed in UC patients (Spearman's ρ=0.40, p=0.029).

Contrary to only 2 UC patients, MES identified 16 (53%) PSC-UC patients with normal endoscopic appearance (MES grade 0; median MES grade 0; Table 2). In the rectum, a similar distribution was observed, with a majority (57%) of PSC-UC patients without histologically active disease (median NHI grade 0, Table 2). However, in the caecum, a more pronounced inflammatory pattern emerged, with 80% of PSC-UC patients displaying NHI grades ranging from 1 to 4 (median NHI grade 2; Table 2). This highlights a significant discrepancy between MES and NHI in PSC-UC patients, which is further corroborated by the lack of correlation between the two measures (Spearman's ρ=0.27, p=0.14). Notably, for the correlation analysis, only the grades corresponding to the most affected lesions were considered, effectively approximating the situation in the caecum (Figure 1, "caecum and rectum").

3.2 MES and NHI in PSC-UC

To understand the discrepancy between MES and NHI in PSC-UC patients, the NHI values of 16 PSC-UC patients with MES grade 0 were analyzed (Figure 2, upper panels). Surprisingly, this analysis revealed that 13 of these patients (81%) had NHI grades between 1 and 4 in the caecum (Figure 3A,B) and 9 (56%) had NHI grades between 1 and 4 in the rectum. When considering both the caecum and rectum for each patient, only 2 individuals (12.5%) had NHI grades of 0 in both segments (Figure 2, "caecum and rectum" panel). Hence, MES failed to detect active UC in 14 (88%) of the PSC-UC patients with MES grade 0, which corresponds to 46% of all PSC-UC patients.

Further analysis of the NHI scores revealed that among the 8 PSC-UC patients with MES grade 1, 3 patients showed no signs of inflammation (NHI grade 0) while 3 exhibited active inflammation with NHI grades ranging from 2 to 4 (Figure 2, middle panels; Figure 3C). Similarly, among the 5 patients with MES grade 2, 2 individuals displayed active inflammation with NHI grade 3 (Figure 2, lower panels; Figure 3D). This suggests that MES incorrectly diagnosed another 3 PSC-UC patients. Taken together, these results clearly indicate that MES insufficiently identified ongoing microscopic inflammation in 17 (57%) of PSC-UC patients, which would negatively affect therapeutic decisions.

3.3 Backwash ileitis and rectal sparing in PSC-UC patients

All patients were characterized as summarized in Table 1. Of note, fecal calprotectin (FC) levels in UC patients were significantly elevated, with a median of 478 µg/g (CI 263–917), compared to the widely accepted upper limit of 100 µg/g[28]. In contrast, FC levels in PSC-UC patients were within the normal range, with a median of 96 µg/g (CI 60-231). This suggests that PSC-

UC patients have nearly absent or very mild UC manifestation, compared to the severe manifestation in UC patients.

Histopathological examination consistently supported the notion of a more severe inflammatory pattern in the rectum of UC patients, as evidenced by the highest NHI grades (Figure 1, Table 2). In contrast, PSC-UC patients predominantly exhibited inflammatory changes in the caecum (median NHI grade 2 vs. 0 in rectum; $p<0.01$; Figure 1; Table 2), suggesting complete or partial rectal sparing. Indeed, 60% of PSC-UC patients had spared rectal mucosa compared to just 10% of UC patients ($p<0.001$).

In addition, inflammation scoring in the ileum exhibited similar median values in both UC and PSC-UC patients (median NHI grade 0; Figure 1, Table 2). Nevertheless, 6 PSC-UC patients (20%) exhibited mild to severe inflammation (NHI grades 1-3) compared to only 1 patient in the UC group (3%; $p=0.047$; Figure 1) thus suggesting higher incidence of backwash ileitis in PSC-UC patients. These findings collectively underscore the variability of inflammation intensity across different segments of the intestines in both PSC-UC and UC.

4. Discussion

Up to now, almost 30 scoring systems have been introduced to accurately assess the colitic disease severity in inflammatory bowel diseases. However, despite extensive validations, none of these systems have been universally recognized as versatile[29]. In this study, we aimed to validate the commonly used MES system for evaluating UC in PSC-UC patients and compare the results with histopathological observations expressed through the NHI. Our findings demonstrate a correlation between MES and NHI in UC patients, but a lack of correlation in PSC-UC patients (as indicated by Spearman's ρ). MES fails to identify ongoing histological inflammation (NHI grade 1-4, Figure 2 and 3) in more than 46% of PSC-UC patients who were assigned MES grade 0. This significant discrepancy highlights a major limitation of endoscopic assessment, which could potentially lead to an underestimation of the severity of PSC-UC. Therefore, we recommend the routine use of histological scoring in clinical practice to overcome this limitation.

It has been reported that UC in PSC manifests mildly or even completely without symptoms compared to typical UC[5, 30]. Additionally, Murasugi et al.[5] documented no correlation between the severity of liver disease and colonic inflammation expressed by MES. They concluded that it is important for colonoscopy to be routinely performed immediately following a diagnosis of PSC. However, our observations show that histopathological evaluation should always accompany colonoscopy to avoid underdiagnosis.

In our current study, the NHI revealed more severe colitis in the caecum of PSC-UC patients, along with an increased occurrence of backwash ileitis and rectal sparing. These findings are consistent with previous studies that have reported a high prevalence of pancolitis in PSC-UC patients, ranging from 80% to 95%, with varying degrees of severity and a pronounced localization in the right-sided colon[4, 5, 7, 30]. Therefore, it is crucial to inspect all

colonic segments (ileum, caecum, rectum, sigmoid, descending, transverse and ascending colon) using both colonoscopy and histopathology to obtain a comprehensive understanding of the disease presentation in PSC-UC patients.

In addition, we suggest that the MES should be evaluated individually for each colonic segment. Lobatón et al.[32], previously developed a modified MES (MMES) that takes into account the extent and severity of endoscopic activity in UC. While the MMES is complex and informative, our experience indicates that it is more suitable for use in clinical trials rather than in everyday clinical practice. Therefore, we propose that MES scores, along with NHI expressed separately for each colonic segment, serve as ideal and informative prognostic factors for assessing complex disease activity.

Although NHI has not been previously validated for PSC-UC, it has been validated for UC[26]. Furthermore, it has shown a good correlation with other established indices such as the Geboes score and global visual analog scale[24]. Given this correlation, we have successfully employed NHI to evaluate the microscopic disease activity in PSC-UC. Importantly, interpretation must be exercised cautiously especially in treated patients, as NHI grade 0 is assigned to both normal histological observation and a mild chronic inflammation without activity.

In conclusion, our study highlights the limited validity of the standard MES scoring system in the context of PSC-UC. Although our study involved a small number of patients from a single center, it emphasizes the importance of incorporating histological evaluation into the diagnostic and grading system for PSC and PSC-UC. Early diagnosis is crucial for the overall clinical management of patients, particularly in terms of monitoring malignant complications and determining the need for orthotopic liver transplantation. Therefore, we recommend that the MES scoring system be reserved for assessing the endoscopic disease activity of UC without

PSC, while histological evaluation should be considered an essential component in the UC diagnosis of PSC and PSC-UC patients.

Acknowledgments

We thank Lenka Bruhova and Katerina Dvorakova for their excellent support. We are especially grateful to all the patients participating in this study.

Author Contributions

Pa.W. designed the study; T.H., L.B., P.D., Pe.W., M.H. recruited and treated patients, collected and analyzed data; O.F. performed histological evaluations; P.B. analyzed data; M.K. performed statistical analyses; all authors interpreted data; Pa.W., A.K., M.G. wrote the manuscript.

References

1. Chapman RW, Arborgh BA, Rhodes JM, et al. Primary sclerosing cholangitis: a review of its clinical features, cholangiography, and hepatic histology. Gut. 1980;21(10):870-7. Epub 1980/10/01.

2. Loftus EV, Jr., Harewood GC, Loftus CG, et al. PSC-IBD: a unique form of inflammatory bowel disease associated with primary sclerosing cholangitis. Gut. 2005;54(1):91-6. Epub 2004/12/14.

3. Weismuller TJ, Trivedi PJ, Bergquist A, et al. Patient Age, Sex, and Inflammatory Bowel Disease Phenotype Associate With Course of Primary Sclerosing Cholangitis. Gastroenterology. 2017;152(8):1975-84 e8. Epub 2017/03/10.

4. Jorgensen KK, Grzyb K, Lundin KE, et al. Inflammatory bowel disease in patients with primary sclerosing cholangitis: clinical characterization in liver transplanted and nontransplanted patients. Inflamm Bowel Dis. 2012;18(3):536-45. Epub 2011/04/02.

5. Murasugi S, Ito A, Omori T, et al. Clinical Characterization of Ulcerative Colitis in Patients with Primary Sclerosing Cholangitis. Gastroenterol Res Pract. 2020;2020:7969628. Epub 2020/11/24.

6. Boonstra K, van Erpecum KJ, van Nieuwkerk KM, et al. Primary sclerosing cholangitis is associated with a distinct phenotype of inflammatory bowel disease. Inflamm Bowel Dis. 2012;18(12):2270-6. Epub 2012/03/13.

7. de Vries AB, Janse M, Blokzijl H, et al. Distinctive inflammatory bowel disease phenotype in primary sclerosing cholangitis. World J Gastroenterol. 2015;21(6):1956-71. Epub 2015/02/17.

8. Mahmoud R, Shah SC, Ten Hove JR, et al. No Association Between Pseudopolyps and Colorectal Neoplasia in Patients With Inflammatory Bowel Diseases. Gastroenterology. 2019;156(5):1333-44 e3. Epub 2018/12/12.

9. Loftus EV, Jr., Sandborn WJ, Lindor KD, et al. Interactions between chronic liver disease and inflammatory bowel disease. Inflamm Bowel Dis. 1997;3(4):288-302. Epub 1997/01/01.

10. Weismuller TJ, Wedemeyer J, Kubicka S, et al. The challenges in primary sclerosing cholangitis--aetiopathogenesis, autoimmunity, management and malignancy. J Hepatol. 2008;48 Suppl 1:S38-57. Epub 2008/02/29.

11. Sokol H, Cosnes J, Chazouilleres O, et al. Disease activity and cancer risk in inflammatory bowel disease associated with primary sclerosing cholangitis. World J Gastroenterol. 2008;14(22):3497-503. Epub 2008/06/21.

12. Kornfeld D, Ekbom A, Ihre T. Is there an excess risk for colorectal cancer in patients with ulcerative colitis and concomitant primary sclerosing cholangitis? A population based study. Gut. 1997;41(4):522-5. Epub 1997/12/10.

13. Broome U, Lofberg R, Veress B, et al. Primary sclerosing cholangitis and ulcerative colitis: evidence for increased neoplastic potential. Hepatology. 1995;22(5):1404-8. Epub 1995/11/01.

14. Maaser C, Sturm A, Vavricka SR, et al. ECCO-ESGAR Guideline for Diagnostic Assessment in IBD Part 1: Initial diagnosis, monitoring of known IBD, detection of complications. J Crohns Colitis. 2019;13(2):144-64. Epub 2018/08/24.

15. Bouguen G, Levesque BG, Pola S, et al. Feasibility of endoscopic assessment and treating to target to achieve mucosal healing in ulcerative colitis. Inflamm Bowel Dis. 2014;20(2):231-9. Epub 2013/12/20.

16. D'Haens G, Sandborn WJ, Feagan BG, et al. A review of activity indices and efficacy end points for clinical trials of medical therapy in adults with ulcerative colitis. Gastroenterology. 2007;132(2):763-86. Epub 2007/01/30.

17. Schroeder KW, Tremaine WJ, Ilstrup DM. Coated oral 5-aminosalicylic acid therapy for mildly to moderately active ulcerative colitis. A randomized study. N Engl J Med. 1987;317(26):1625-9. Epub 1987/12/24.

18. Sandborn WJ, Feagan BG, Hanauer SB, et al. A review of activity indices and efficacy endpoints for clinical trials of medical therapy in adults with Crohn's disease. Gastroenterology. 2002;122(2):512-30. Epub 2002/02/08.

19. Park S, Abdi T, Gentry M, et al. Histological Disease Activity as a Predictor of Clinical Relapse Among Patients With Ulcerative Colitis: Systematic Review and Meta-Analysis. Am J Gastroenterol. 2016;111(12):1692-701. Epub 2016/10/12.

20. Ozaki R, Kobayashi T, Okabayashi S, et al. Histological Risk Factors to Predict Clinical Relapse in Ulcerative Colitis With Endoscopically Normal Mucosa. J Crohns Colitis. 2018;12(11):1288-94. Epub 2018/06/26.

21. Lemmens B, Arijs I, Van Assche G, et al. Correlation between the endoscopic and histologic score in assessing the activity of ulcerative colitis. Inflamm Bowel Dis. 2013;19(6):1194-201. Epub 2013/03/23.

22. Bryant RV, Burger DC, Delo J, et al. Beyond endoscopic mucosal healing in UC: histological remission better predicts corticosteroid use and hospitalisation over 6 years of follow-up. Gut. 2016;65(3):408-14. Epub 2015/05/20.

23. Zenlea T, Yee EU, Rosenberg L, et al. Histology Grade Is Independently Associated With Relapse Risk in Patients With Ulcerative Colitis in Clinical Remission: A Prospective Study. Am J Gastroenterol. 2016;111(5):685-90. Epub 2016/03/16.

24. Mosli MH, Parker CE, Nelson SA, et al. Histologic scoring indices for evaluation of disease activity in ulcerative colitis. Cochrane Database Syst Rev. 2017;5:CD011256. Epub 2017/05/26.

25. Marchal-Bressenot A, Salleron J, Boulagnon-Rombi C, et al. Development and validation of the Nancy histological index for UC. Gut. 2017;66(1):43-9. Epub 2015/10/16.

26. Marchal-Bressenot A, Scherl A, Salleron J, et al. A practical guide to assess the Nancy histological index for UC. Gut. 2016;65(11):1919-20. Epub 2016/08/28.

27. Magro F, Doherty G, Peyrin-Biroulet L, et al. ECCO Position Paper: Harmonization of the Approach to Ulcerative Colitis Histopathology. J Crohns Colitis. 2020;14(11):1503-11. Epub 2020/06/07.

28. Bjarnason I. The Use of Fecal Calprotectin in Inflammatory Bowel Disease. Gastroenterol Hepatol (N Y). 2017;13(1):53-6. Epub 2017/04/20.

29. Mohammed Vashist N, Samaan M, Mosli MH, et al. Endoscopic scoring indices for evaluation of disease activity in ulcerative colitis. Cochrane Database Syst Rev. 2018;1(1):CD011450. Epub 2018/01/18.

30. Palmela C, Peerani F, Castaneda D, et al. Inflammatory Bowel Disease and Primary Sclerosing Cholangitis: A Review of the Phenotype and Associated Specific Features. Gut Liver. 2018;12(1):17-29. Epub 2017/04/05.

31. Wohl P, Hucl T, Drastich P, et al. Epithelial markers of colorectal carcinogenesis in ulcerative colitis and primary sclerosing cholangitis. World J Gastroenterol. 2013;19(14):2234-41. Epub 2013/04/20.

32. Lobaton T, Bessissow T, De Hertogh G, et al. The Modified Mayo Endoscopic Score (MMES): A New Index for the Assessment of Extension and Severity of Endoscopic Activity in Ulcerative Colitis Patients. J Crohns Colitis. 2015;9(10):846-52. Epub 2015/06/28.

Table 1. Characterization of patients.

	UC	PSC-UC	p
Patients, *n*	29	30	-
Sex (male), *n* (%)	16 (55)	23 (77)	0.10
Age (years), mean ± SD	43.2 ± 12.5	37.2 ± 2.9	0.07
Duration of disease (years), mean ± SD	12.9 ± 10.6	10.6 ± 6.9	0.62
pANCA positive, *n* (%)	14 (48)	16 (53)	0.8
Portal hypertension, *n*	0	0	-
Cholecystectomy, *n* (%)	1 (3)	1 (3)	-
BMI (a. u.), mean ± SD	25.1 ± 4.1	23.5 ± 4.2	0.1
Corticosteroids, *n* (%)	10 (34)	10 (33)	-
Mesalamine, *n* (%)	12 (41)	20 (66)	-
Mesalamine and immunomodulators, *n* (%)	12 (41)	9 (30)	-
Biological treatment, *n* (%)	5 (17)	0	-
Ursodeoxycholic acid, *n* (%)	0	30 (100)	-
Fecal calprotectin (µg/g), median (95% CI)	478 (263–917)	96 (60-231)	<0.001

UC, ulcerative colitis; PSC-UC, primary sclerosing cholangitis with concomitant ulcerative colitis; pANCA, perinuclear anti-neutrofil cytoplasm autoantibodies; BMI, body mass index; a.u., arbitrary units; SD, standard deviation; CI, confidence interval

Table 2. Calculated medians (95% CI) of MES and NHI.

	PSC-UC	UC	p
MES	0 (0-1)	2 (1-2)	<0.001
inflammation (ileum)	0 (0-0)	0 (0-0)	-
NHI (caecum)	2 (1-2)	1 (0-2)	0.048
NHI (rectum)	0 (0-1)	2 (0-3)	0.002

CI, confidence interval; MES, Mayo endoscopic subscore; NHI, Nancy histological index; PSC-UC, primary sclerosing cholangitis with concomitant ulcerative colitis; UC, ulcerative colitis

Figure legends

Figure 1. MES, NHI and inflammation grade of PSC-UC and UC patients in the caecum, rectum and ileum. 'Caecum and rectum' panels represent only the most severely affected lesions for each patient. The numbers of patients per grade are indicated in the graph.

Figure 2. NHI scores of PSC-UC patients with MES grade 0 (top panels), MES grade 1 (middle panels) and MES grade 2 in the caecum and rectum. 'Caecum and rectum' panels represent only the most severely affected lesions for each patient. The numbers of patients per grade are indicated in the graph.

Figure 3. Hematoxylin-eosin stained caecal biopsies from PSC-UC patients with MES grade 0 (A, B), MES grade 1 (C), and MES grade 2 (D). All samples show an active colitic pattern with numerous neutrophils infiltrated into lamina propria and epithelium accompanied by ulceration (A) and crypt abscesses (B-D). Samples were thus assigned NHI grades 4 (A) and 3 (B-D). Scale bar, 50 μm.

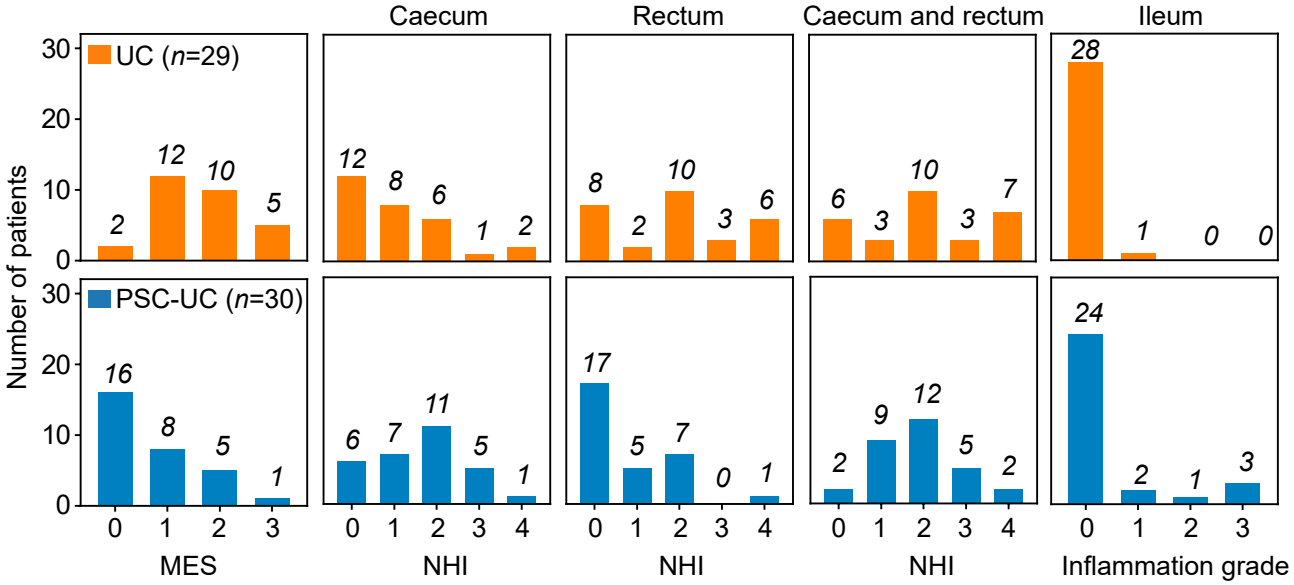

Figure 1

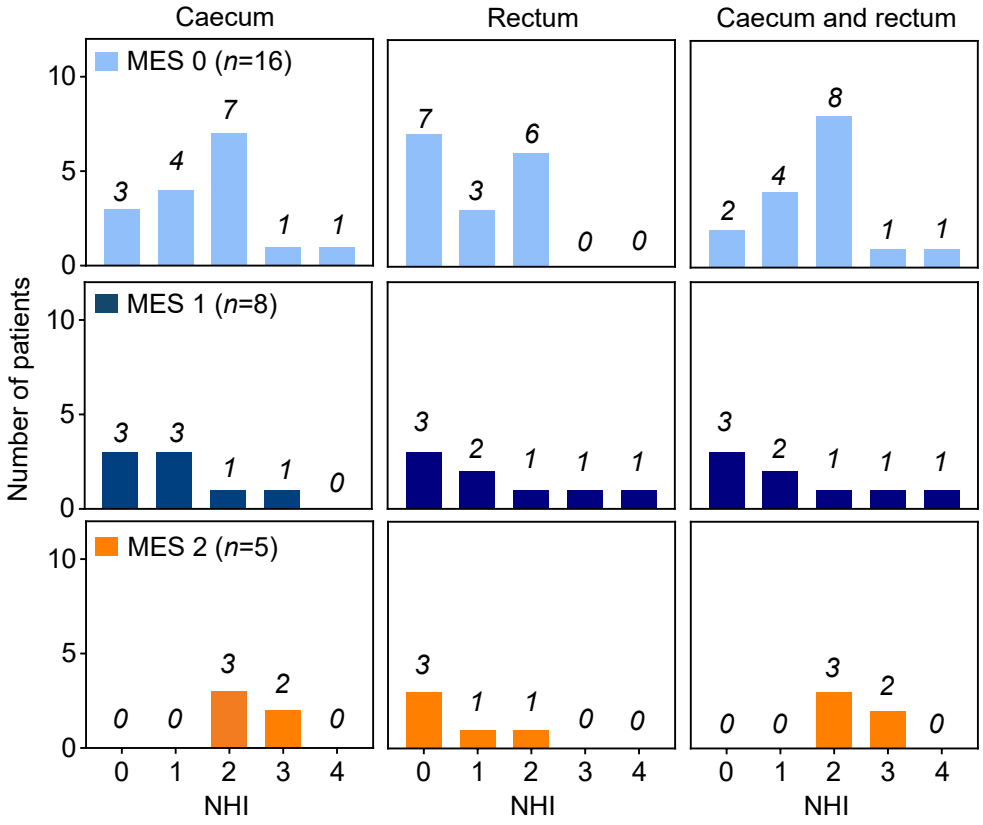

Figure 2

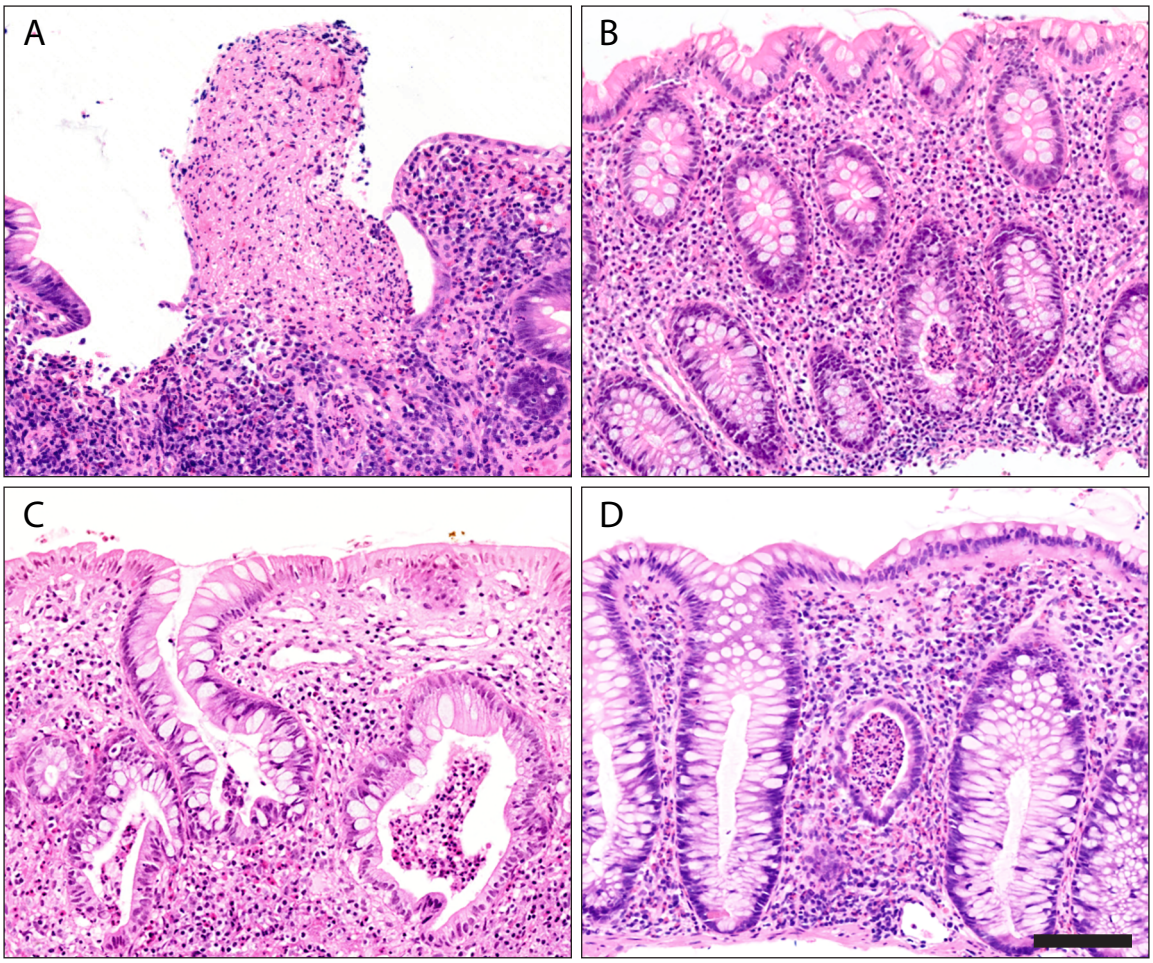

Figure 3